J. Fluid Mech. (1992), *vol.* 243, *pp.* 319–351
Printed in Great Britain

On a degeneracy of temporal secondary instability modes in Blasius boundary-layer flow

By W. KOCH
DLR Institute for Theoretical Fluid Mechanics, D-3400 Göttingen, Germany

(Received 31 October 1991 and in revised form 21 March 1992)

Using the parallel-flow approximation the prechaotic bifurcation behaviour of Blasius boundary-layer flow is studied at finite Reynolds numbers. The objective of this investigation is to search for qualitative solution changes which might be linked to the rapid breakdown at transition. As a first step this requires the computation of the two-dimensional primary equilibrium surface of nonlinear Tollmien–Schlichting waves. This two-dimensional neutral surface exhibits a period-halving bifurcation which is qualitatively different from the situation for plane Poiseuille flow. At the same time the numerically computed equilibrium solution offers the possibility of assessing the range of convergence of weakly nonlinear results.

In a second step the stability of this nonlinear equilibrium solution is investigated with respect to three-dimensional disturbances. Of particular importance is the existence of a modal degeneracy between amplified secondary instability modes, implying locally algebraic growth. On decreasing the Reynolds number, the amplification rate of this direct resonance point switches from being amplified to being damped. Interestingly, the Reynolds number corresponding to this zero-amplification point seems to be in the vicinity of the experimentally observed transition Reynolds number for Blasius flow.

1. Introduction

Many physically interesting and technologically important fluid-mechanical phenomena have their origin in the nonlinearity of the governing Navier–Stokes equations. For example, the transition from smooth and ordered laminar flow to the random and chaotic motion of turbulent flow is such a fundamental nonlinear problem which also motivated the present investigation. An up-to-date survey of the physical processes during transition and their mathematical modelling together with additional references can be found in Morkovin's (1991) lucid overview. Only fairly recent advances in highly nonlinear large-Reynolds-number theory, numerical methods, computing facilities and experimental techniques have made it possible to shed some light on the highly nonlinear advanced stages of transition. But even so, present-day computer resources and algorithms limit our computations to rather simple model problems at relatively low Reynolds numbers. Many questions, in particular at supersonic and hypersonic speeds, remain unanswered and are the subject of ongoing intensive research. It is hoped that this research effort will not only result in a better physical understanding of the transition process, but will also provide a more rational practical transition prediction method to supersede the semi-empirical techniques currently used in engineering applications.

The relevant nonlinear theoretical studies may be divided roughly into two

categories, namely expansion methods and numerical computations of the full Navier–Stokes equations. Based upon analytical theories the *expansion methods* rely on the assumption of a vanishingly small expansion parameter such as the disturbance amplitude or the inverse Reynolds number (see for example the monograph by Drazin & Reid (1981) for an introductory survey or Smith's (1979*a*, *b*) self-consistent high-Reynolds-number approach. Recently Smith and his colleagues, cf. Smith (1991) for a brief survey, have developed the high-Reynolds-number approach into a truly nonlinear theory for which the mean-flow profile is completely altered from its original form). Naturally, expansion methods also require numerical computations, but in general they have to be performed for simpler equations. A mathematically more rigorous derivation of weakly nonlinear amplitude equations is possible via the locally valid methods of *dynamical systems theory* (centre-manifold theory, normal form theory and local equivariant dynamical systems theory, see for example Guckenheimer & Holmes 1983). In these studies degenerate bifurcation points are often used to capture, in a local analysis, the global behaviour that is observed in full numerical simulations far from this bifurcation point, e.g. Mahalov & Leibovich (1991).

The second category comprises methods which require solution of the full Navier–Stokes equations. At the expense of much higher computational complexity the corresponding global solutions have no limitation as far as the expansion parameter is concerned, but computer storage and time requirements still prohibit application at large Reynolds numbers. Here Smith's highly nonlinear theory could provide a viable alternative. The methods of this second category may be subdivided further into direct numerical simulations and numerical bifurcation approaches. *Direct numerical simulations* (see the recent overview by Kleiser & Zang 1991) follow the time-accurate evolution of initially prescribed disturbances by solving the initial-boundary-value problem. The recently derived *parabolic stability equations*, cf. Bertolotti (1991*a*, *b*) or Chang *et al.* (1991), considerably reduce the computational cost of direct numerical simulations by parabolizing the governing equations in the streamwise direction for slowly varying flows like boundary layers. The approximate results obtained show excellent agreement with full numerical simulations up to the highly nonlinear 'spike' stage. Contrary to direct numerical simulation or parabolic stability theory the goal of *numerical bifurcation theory*, the approach to be employed in the present investigation, is to locate qualitative solution changes directly and trace these changes in the parameter space by solving a boundary-value problem.

The equilibrium solutions of numerical bifurcation theory are special solutions like stationary, time-periodic or at most quasi-periodic solutions. Contrary to direct numerical simulation, chaotic attracting states cannot be handled yet, limiting our bifurcation solutions to prechaotic states. Of particular importance is the stability of these equilibrium states. If they are stable, they describe attracting states of the solution evolving in time. In a certain parameter range this is the case for various closed-flow problems such as Taylor–Couette or Rayleigh–Bénard flow. Therefore most applications of numerical bifurcation theory are found for closed-flow problems, a typical example being the work of Cliffe (1988).

In open flows like Poiseuille flow, Blasius boundary-layer flow or flows past more complicated aerodynamic configurations, these equilibrium states are apparently unstable in most cases and therefore extremely difficult to trace in experiments or direct numerical simulations. Yet, there appears to be a possible connection between these unstable equilibrium states and the large-scale coherent structures observed in transitional and turbulent flows (cf. Saffman 1983). This adds new importance to

these prechaotic equilibrium solutions and one hopes that they will provide clues for more rational practical transition criteria in flows controlled by large-scale coherent structures (cf. Ehrenstein & Koch 1991).

Exactly parallel flows such as plane Poiseuille flow admit time-periodic equilibrium solutions which have the form of spatially periodic finite-amplitude waves (cf. for example Herbert 1977, Barkley 1990, Bridges 1991, or Ehrenstein & Koch 1991). These spatially periodic waves allow a considerably simplified numerical treatment because one needs to resolve only one wavelength. In external flows like Blasius boundary-layer flow, the time-periodic equilibrium solutions are no longer exactly periodic in the streamwise direction and additional complications are encountered with inflow and outflow boundary conditions, compare Fasel's (1976) work. In particular the proper outflow boundary conditions are still an unresolved question.

While these difficulties have to be coped with in future bifurcation studies for flows past blunt bodies, one usually makes the simplifying parallel-flow assumption for flows past streamlined bodies. In this approximation the boundary-layer growth is suppressed locally by introducing a fictitious body force in the streamwise direction which makes the asymptotic boundary-layer profile an exact solution of the steady Navier–Stokes equations. The relevance of this approximation remains to be assessed by full non-parallel computations in particular at low Reynolds numbers. But for the time being this commonly used artifice allows us to study nonlinear, spatially periodic wave-like equilibrium solutions in boundary-layer flows. Encouraged by the excellent results obtained with temporal simulations (see Kleiser & Zang 1991) we believe that the corresponding bifurcation results are meaningful approximations of the non-parallel solution.

As pointed out by Soibelman & Meiron (1991) in their bifurcation analysis of plane Poiseuille flow, a major advantage of the time-dependent numerical approach is the availability of high-resolution numerics, enabling it to simulate experimentally observed flows, cf. Kleiser & Zang (1991). On the other hand the numerical bifurcation approach leads to large systems of nonlinear algebraic equations, the efficient numerical treatment of which is still in a rather unsatisfactory state, limiting this approach to low-resolution studies. The main advantage of the bifurcation approach is the capability of computing unstable solutions of a specified form. Also the solution can be varied easily in parameter space. While the generally insufficient resolution severely hampers the accuracy of bifurcation solutions, it turns out that often few modes are sufficient to give a good qualitative and sometimes even quantitative result.

Therefore the main objective of this investigation is a search for qualitative changes in equilibrium solutions which might offer an explanation for the explosive character of transition. For this purpose we compute in §2 first the two-dimensional neutral surface of finite-amplitude travelling waves in a Blasius boundary layer (primary equilibrium surface). Even using the parallel-flow approximation only very few high-amplitude results exists, i.e. Milinazzo & Saffman (1985), Lifshits & Shtern (1986) or Lifshits, Rakhmatullaev & Shtern (1989), to name the three publications known to the author. To a certain extent the travelling-wave calculations of Conlisk, Burggraf & Smith (1987) based on the nonlinear triple-deck equations also belong to this group. One property distinguishing the two-dimensional neutral surface for Blasius flow from the hitherto published results for plane Poiseuille flow is the existence of a two-dimensional *period-halving bifurcation* which has been described so far only by Lifshits *et al.* (1989). (In a private communication F. T. Smith pointed out that this bifurcation was anticipated by him (Smith 1988) as a possibility in the

form of a nonlinear 'breakdown' which tends to be confirmed by the follow-up work of Smith & Khorrami (1991) on an analogous problem). These two-dimensional bifurcations occur at fairly high amplitudes making them physically less important than the three-dimensional solutions originating at the now classical fundamental (Klebanoff type) or subharmonic (Craik/Herbert type) secondary instability, cf. Herbert (1988).

The stability computation of the two-dimensional equilibrium solutions with respect to these three-dimensional disturbances represents the second step in our investigation and is treated in §3. The main difference to Herbert's (1988) fairly exhaustive studies is that we use the 'exact' two-dimensional equilibrium solution and do not need to employ the shape assumption. This allows us to study the stability at higher amplitudes of the two-dimensional neutral solution also and not only near threshold. One particularly noteworthy finding is the existence of a modal degeneracy between secondary instability modes. Such a modal coalescence, frequently termed a direct resonance, has been studied extensively in linearized primary instability problems (see for example Benney & Gustavsson 1981; Koch 1986; Jones 1988; Shanthini 1989, and references cited in these papers). A striking difference between the direct resonance for primary instabilities and our secondary instability degeneracy is that the former involve only damped modes while we obtained coalescence between amplified modes which already sustain themselves in the linear analysis.

Exact direct resonances occur only at discrete points in parameter space and imply locally algebraic growth. The corresponding comparatively explosive growth appears to provide a possible mechanism to explain theoretically the abrupt changes observed during transition. It is interesting to note that in a similar approach, but using a prescribed mean turbulent profile instead of our equilibrium solution, Jang, Benney & Gran (1986) argue that a direct resonance might be the possible reason for the appearance of streamwise vorticities in a turbulent boundary layer. However, being aware of the non-uniqueness of the transition process, see Morkovin (1991), direct resonance of phase-locked Klebanoff-type fundamental modes can be at most one of several mechanisms, particularly since vital ingredients of transition such as receptivity are still to be included. Therefore this study should be considered only as an attempt to shed more light on the nonlinear bifurcation structure of boundary-layer flows. To clarify the implications of the modal degeneracy on the transition process certainly requires further more penetrating studies. Also one needs to investigate to what extent non-parallelity of the flow alters these finite-Reynolds number results, cf. Smith (1979*a*).

2. Two-dimensional neutral surface solution

2.1. *Governing equations*

We consider the flow of an incompressible viscous fluid of constant kinematic viscosity ν^* past a semi-infinite flat plate located at

$$y^* = 0, \quad 0 \leqslant x^*, \quad -\infty < z^* < +\infty.$$

All quantities are non-dimensionalized with the laminar free-stream velocity U_∞^* and the self-similarity reference length $L^* = (\nu^* x^*/U_\infty^*)^{\frac{1}{2}}$. Then $\boldsymbol{x} \equiv (x, y, z) = \boldsymbol{x}^*/L^*$ is the non-dimensional Cartesian coordinate vector with components in the streamwise, normal and spanwise direction, and $\boldsymbol{v} \equiv (u, v, w) = \boldsymbol{v}^*/U_\infty^*$ denotes the corresponding

dimensionless velocity vector. If only two-dimensional disturbances are considered, a stream function $\psi(x, y)$ can be introduced:

$$u = \partial\psi/\partial y, \quad v = -\partial\psi/\partial x, \tag{1}$$

such that the governing equations of motion can be written

$$\left\{\frac{\partial}{\partial t}+\frac{\partial\psi}{\partial y}\frac{\partial}{\partial x}-\frac{\partial\psi}{\partial x}\frac{\partial}{\partial y}-\frac{1}{Re}\nabla^2\right\}\nabla^2\psi = F(x, y, t). \tag{2}$$

Here $Re = (x^*U_\infty^*/\nu^*)^{\frac{1}{2}}$ is the Reynolds number and F denotes a body force which will be chosen such as to make the quasi-parallel boundary-layer profile an exact solution of the Navier–Stokes equations. On the flat plate the no-slip boundary condition has to be satisfied and at infinity proper decay conditions have to be imposed.

For the following two-dimensional analysis we may split the solution into two parts

$$\psi(x, y, t) = \Psi(x, y)+\epsilon_{2D}\tilde{\psi}(x, y, t), \tag{3}$$

where $\Psi(x, y)$ denotes a steady laminar solution of (2) while $\tilde{\psi}(x, y, t)$ contains the fluctuating part. ϵ_{2D} is a conveniently chosen amplitude of arbitrary size. Avoiding the difficult (numerical) computation of the exact two-dimensional laminar flow $\Psi(x, y)$ we fix L^* (and hence Re) and select the local quasi-parallel Blasius boundary-layer flow $U(x, y) = f'(y)$, $V(x, y) = 0$ as our basic laminar flow. The function $f(y)$ is the solution of the Blasius equation

$$2f'''+ff'' = 0, \tag{4}$$

with $f(0) = f'(0) = 0$ and $f'(\infty) = 1$. Naturally the Blasius solution is not an exact solution of the Navier–Stokes equations. But substituting the Blasius solution into the equations of motion, the leftover terms can be eliminated formally by choosing the artificial force term F appropriately. The physical relevance of this *ad hoc* procedure still has to be ascertained by an exact non-parallel computation in the spirit of Fasel's (1976) work. At present however the parallel-flow assumption leads to a considerable reduction in the numerical computation and seems to be adequate for our purposes.

Fixing L^* does not necessarily mean that the free-stream mean velocity of the time-dependent nonlinear solution remains equal to U_∞^*. This subtle point has also been of major concern in other investigations, cf. Likhachev & Shtern (1975), Smith (1979*b*), Milinazzo & Saffman (1985) or Fischer (1990). A related question in plane Poiseuille flow is the unique determination of the nonlinear solution by imposing the constant-flux or constant-pressure-gradient condition, see for example Stuart (1960) or Milinazzo & Saffman (1985). To clarify a frequent misunderstanding we emphasize the fact that the time-dependent nonlinear equilibrium solution computed by imposing the constant-pressure-gradient condition is physically different from the constant-flux solution generally realized in plane Poiseuille flow experiments. This does not imply a violation of global balances because these nonlinear equilibrium solutions have been computed under different physical restrictions in parameter space; but these solutions can be related to each other. Only for steady laminar flow do the two solutions coincide.

In the following we concentrate on wave-like solutions which are rather special time-periodic solutions, being nonlinear extensions of the classical linear Tollmien–Schlichting waves. In a frame of reference $x' = x-Ct$ moving with the (unknown) wave speed C the nonlinear solution is stationary ($\partial/\partial t \equiv 0$) and periodic in the

streamwise direction. Writing from now on x instead of x', $\tilde{\psi}$ may be expressed as a Fourier series in the streamwise direction

$$\tilde{\psi}(x,y) = \sum_{n=-\infty}^{\infty} \hat{\psi}_n(y) \exp(in\alpha x), \tag{5}$$

with α being the streamwise wavenumber. Reality of the solution requires $\hat{\psi}_{-n}(y) = \bar{\hat{\psi}}_n(y)$, where the bar denotes the complex conjugate. As a consequence we need to solve only for $n \geqslant 0$. Substituting (5) into (2) and equating equal exponentials we obtain the modal equations for $n \geqslant 0$

$$\left\{\frac{1}{Re} \mathrm{D}_n^2 - in\alpha[U(y)-C]\,\mathrm{D}_n + in\alpha \frac{\mathrm{d}^2 U}{\mathrm{d}y^2}\right\}\hat{\psi}_n - \epsilon_{2\mathrm{D}} \sum_{\nu=-\infty}^{\infty} N_{n-\nu,\nu} = 0, \tag{6}$$

with the convolution term

$$N_{\mu,\nu} = i\alpha\left\{\mu \frac{\mathrm{d}\hat{\psi}_\nu}{\mathrm{d}y} \mathrm{D}_\mu \hat{\psi}_\mu - \nu \hat{\psi}_\nu \mathrm{D}_\mu \frac{\mathrm{d}\hat{\psi}_\mu}{\mathrm{d}y}\right\}, \quad \mathrm{D}_n = \mathrm{d}^2/\mathrm{d}y^2 - (n\alpha)^2. \tag{7}$$

For $n = 0$ the relevant equation may be integrated once with respect to y. As demonstrated by Herbert (1977) the corresponding constant of integration implies a change of the mean pressure gradient in the streamwise direction and is therefore equal to zero in our formulation. $\hat{\psi}_0$ appears only as derivative, i.e. $\mathrm{d}\hat{\psi}_0/\mathrm{d}y = \hat{u}_0$, such that the modal equations (6) can be rewritten

$$n = 0: \quad \frac{1}{Re}\frac{\mathrm{d}^2 \hat{u}_0}{\mathrm{d}y^2} + 2\alpha\epsilon_{2\mathrm{D}} \operatorname{Im}\left\{\sum_{\nu=1}^{\infty} \nu \bar{\hat{\psi}}_\nu \frac{\mathrm{d}^2 \hat{\psi}_\nu}{\mathrm{d}y^2}\right\} = 0, \tag{8}$$

$$n > 0: \quad \left\{\frac{1}{Re} \mathrm{D}_n^2 - in\alpha[U(y)-C]\,\mathrm{D}_n + in\alpha \frac{\mathrm{d}^2 U}{\mathrm{d}y^2}\right\}\hat{\psi}_n$$

$$- i\epsilon_{2\mathrm{D}} n\alpha\left\{\hat{u}_0 \mathrm{D}_n \hat{\psi}_n - \hat{\psi}_n \frac{\mathrm{d}^2 \hat{u}_0}{\mathrm{d}y^2}\right\} - \epsilon_{2\mathrm{D}} \sum_{\nu=-\infty}^{\infty}{}'' N_{n-\nu,\nu} = 0. \tag{9}$$

Here Σ'' denotes the sum in (6) without the $N_{0,n}$ and $N_{n,0}$ terms.

The no-slip boundary conditions on the plate are simply

$$n = 0: \quad \hat{u}_0(y=0) = 0, \tag{10}$$

$$n > 0: \quad \hat{\psi}_n(y=0) = \mathrm{d}\hat{\psi}_n/\mathrm{d}y(y=0) = 0. \tag{11}$$

At infinity we require all disturbances to decay, with the exception of $\hat{u}_0$ which remains finite as $y \to \infty$ (compare Likhachev & Shtern 1975). Based upon the more general expansion procedure of Eckhaus (1965), which contrary to the classical Stuart (1960) approach does not separate *a priori* time and wall-normal coordinate in the expansion coefficients, Fischer (1990) was able to show that in the limit as $t \to \infty$ the weakly nonlinear solution requires a finite mean flow deformation $\hat{u}_0(\infty) \neq 0$ at infinity. (This is a consequence of the parallel-flow assumption. If non-parallel flow effects are included, as in Smith (1979*b*), the mean flow deformation $\hat{u}_0$ decays at infinity.) Fischer (1990) therefore suggested using the Neumann condition

$$\mathrm{d}\hat{u}_0/\mathrm{d}y \to 0 \quad \text{as} \quad y \to \infty \tag{12}$$

which will be also employed in this investigation. This is analogous to plane Poiseuille flow, where the constant-pressure-gradient solution of the nonlinear periodic state results in a mean velocity at midchannel which differs from that of

laminar flow but has a vanishing derivative at midchannel. Finally, to fix the phase and the amplitude ϵ_{2D} a local normalization condition will be imposed as defined in (21).

2.2. *Numerical solution procedure*

To solve the modal equations (8) and (9) numerically we convert them into algebraic form via Chebychev collocation. For this purpose we map the semi-infinite domain $y \in [0, \infty)$ into $\eta \in [1, 0)$ by means of the exponential transformation

$$\eta = \exp(-y/y_0), \quad y = y_0 \ln \eta. \tag{13}$$

While Boyd (1989) makes some cautioning remarks, Spalart (1984) and Laurien & Kleiser (1989) have used this transformation with obvious success if y_0 is chosen large enough. Selecting $y_0 = 15$ we truncate the modal expansion (5) at $n = N$, where $N \leqslant 6$ in our computations.

As demonstrated by Herbert (1977) and Ehrenstein & Koch (1991) the modal equations (8) and (9) possess certain symmetry properties in the η-plane (assuming a symmetric continuation of the Blasius profile for $-1 \leqslant \eta < 0$ and that the collocation points have been chosen symmetrically about $\eta = 0$). Of particular importance is the symmetric solution

$$\hat{u}_0^{(s)}(-\eta) = \hat{u}_0^{(s)}(+\eta), \quad \hat{\psi}_n^{(s)}(-\eta) = (-1)^{n+1}\hat{\psi}_n^{(s)}(+\eta), \tag{14}$$

which reduces to the linearly unstable symmetric mode $\hat{\psi}_1(\eta)$ for $\epsilon_{2D} = 0$. Extending this symmetric solution to $\epsilon_{2D} > 0$, $\hat{u}_0(\eta)$ as well as each Fourier mode

$$\hat{\psi}_n(\eta), \quad 1 \leqslant n \leqslant N$$

(denoted collectively by $\hat{q}(\eta)$) is expanded in terms of the relevant even or odd Chebsyshev polynomials in the half-domain $0 \leqslant \eta \leqslant 1$

$$\hat{q}^{\text{even}}(\eta) = \sum_{k=0}^{K-1} a_{2k} T_{2k}(\eta), \quad \hat{q}^{\text{odd}}(\eta) = \sum_{k=0}^{K-1} a_{2k+1} T_{2k+1}(\eta). \tag{15}$$

$T_k(\eta) = \cos(k \cos^{-1}\eta)$ is the kth-order Chebyshev polynomial and the modal values of $\hat{u}_0$ and $\hat{\psi}_n$ at the K collocation points

$$\eta_j = \cos[j\pi/(2K-1)], \quad j = 0, \ldots, K-1, \tag{16}$$

are denoted by

$$\hat{u}_{0j} = \hat{u}_0(\eta_j) = \hat{u}_0(y_j); \quad \hat{\psi}_{nj} = \hat{\psi}_n(\eta_j) = \hat{\psi}_n(y_j), \quad 1 \leqslant n \leqslant N, \quad 0 \leqslant j \leqslant K-1. \tag{17}$$

The pth derivative in the transformed η-plane can be computed by the matrix collocation method (cf. Gottlieb, Hussaini & Orszag 1984),

$$\mathrm{d}^p \hat{q}(\eta_j)/\mathrm{d}\eta^p = \sum_{k=0}^{K-1} \hat{\mathrm{D}}_{jk}^{(p)} \hat{q}(\eta_k), \quad 0 \leqslant j \leqslant K-1. \tag{18}$$

Depending upon the symmetry of $\hat{q}(\eta)$, $\hat{\mathrm{D}}_{jk}$ is either the symmetric or antisymmetric derivative matrix

$$\hat{\mathrm{D}}_{jk}^{(s)} = \mathrm{D}_{jk} + \mathrm{D}_{j,\,2K-1-k}, \quad \hat{\mathrm{D}}_{jk}^{(a)} = \mathrm{D}_{jk} - \mathrm{D}_{j,\,2K-1-k}, \quad 0 \leqslant j \leqslant K-1, \tag{19}$$

where D_{jk}, with $\mathrm{D}_{jk}^{(p)} = (\mathrm{D}_{jk})^p$, is the derivative matrix in the full domain,

$$-1 \leqslant \eta \leqslant +1,$$

given by Gottlieb *et al.* (1984). In the physical y-plane

$$\mathrm{d}^p \hat{q}(y_j)/\mathrm{d}y^p = \sum_{k=0}^{K-1} \tilde{\mathrm{D}}_{jk}^{(p)} \hat{q}(y_k), \quad 0 \leqslant j \leqslant K-1, \tag{20}$$

with $\tilde{\mathrm{D}}_{jk} = \hat{\mathrm{D}}_{jk}\, m(y_j)$ where $m = \partial\eta/\partial y$ denotes the metric of the transformation. Higher derivatives are obtained by applying the chain rule.

Observing the symmetry of each mode, cf. (14), the boundary conditions at infinity are fulfilled automatically. To satisfy the boundary conditions on the plate we follow a method of Ehrenstein (1988): instead of simply replacing suitable rows in the discretization matrix as suggested by Gottlieb *et al.* (1984), this method has the advantage that spurious (unstable) modes are eliminated by splitting the fourth-order differential operator into two second-order operators.

The *local normalization condition*

$$\hat{v}_n(y_{\mathrm{norm}}) \equiv -\mathrm{i}n\alpha\hat{\psi}_n(y_{\mathrm{norm}}) = 1 \tag{21}$$

fixes the phase and amplitude of the solution. In general we choose $n = 1$ and y_{norm} as the tenth collocation point for $K = 30$. This places y_{norm} in the vicinity of the laminar boundary-layer displacement thickness $\delta_1 = 1.720787$ (cf. figure 8). If the first mode is not excited we select $n = 2$.

Substituting (17) and (20) into the normalization condition (21) as well as into the modal equations (8) and (9) (with due consideration of Ehrenstein's 1988 treatment of the boundary conditions), and satisfying them at each internal collocation point we obtain a large system of nonlinear algebraic equations of the form

$$\boldsymbol{F}(\boldsymbol{u}; Re, \alpha) = 0. \tag{22}$$

Here $\boldsymbol{u}$ denotes the solution vector

$$\boldsymbol{u} \equiv \{\hat{u}_{0j}; \mathrm{Re}(\hat{\psi}_{nj}), \mathrm{Im}(\hat{\psi}_{nj}); C, \epsilon_{2\mathrm{D}}\}, \quad 0 < n \leqslant N, \quad 1 \leqslant j \leqslant K-1, \tag{23}$$

containing the unknown modal values at the $K-1$ interior collocation points together with the unknown wave speed C and amplitude $\epsilon_{2\mathrm{D}}$. (Re, α) is the two-dimensional parameter vector and $\mathrm{Re}(z)$ or $\mathrm{Im}(z)$ denote the real or imaginary part of z. In actual computations one parameter, the so-called *control parameter* p, is fixed while the other is the varying *bifurcation parameter* λ. Choosing $\lambda = \alpha$ we obtain $Re =$ constant cuts through the equilibrium surface, while $\alpha =$ constant cuts are computed if $\lambda = Re$.

Individual nonlinear solution branches in cut planes are calculated by pseudo-arclength continuation (cf. Keller 1977). For this purpose a pseudo-arclength parameter s is defined by the parameterizing equation

$$N(\boldsymbol{u}; \lambda, s) \equiv \theta \frac{\mathrm{d}\boldsymbol{u}}{\mathrm{d}s}(s_0) \cdot [\boldsymbol{u}(s) - \boldsymbol{u}(s_0)] + (1-\theta)\frac{\mathrm{d}\lambda}{\mathrm{d}s}(s_0) \cdot [\lambda(s) - \lambda(s_0)] - (s - s_0) = 0. \tag{24}$$

Keller (1977) introduced the tuning factor $0 < \theta < 1$ to place a different emphasis on the solution vector $\boldsymbol{u}$ or the branching parameter λ in order to obtain fairly evenly spaced points along the solution branch. Starting with a known solution at $s = s_0$, which in our case is either a solution on the linear neutral surface or a previously computed nonlinear solution, an initial approximation to the new solution at s can be obtained via the tangent predictor

$$\boldsymbol{u}(s) = \boldsymbol{u}(s_0) + \frac{\partial \boldsymbol{u}}{\partial s}(s_0)\,[s - s_0]. \tag{25}$$

This approximate solution is then corrected by Newton–Raphson iteration of the extended system

$$\boldsymbol{F}(\boldsymbol{u}, \lambda; p) = 0, \quad N(\boldsymbol{u}, \lambda, s) = 0, \tag{26}$$

which converges rapidly for a suitably chosen step size $(s-s_0)$. The extended system above introduced has the advantage that its Jacobian matrix is non-singular at limit points and therefore overcomes the failure of simple parameter continuation in λ at such points. Furthermore, simple bifurcation points can be detected by monitoring the sign of the Jacobian determinant and branch switching methods can be applied. The tangent $\partial \boldsymbol{u}/\partial s(s_0)$ can be found as a simple by-product of the Newton–Raphson iteration.

2.3. *Physical quantities of interest*

Both, mean-flow quantities and fluctuating quantities characterize the nonlinear state. The most obvious mean-flow quantity is the *mean-velocity profile*

$$u_{\mathrm{m}}(y) = f'(y) + \epsilon_{2\mathrm{D}}\,\hat{u}_0(y).$$

As elaborated before, in our constant-pressure-gradient formulation the mean free-stream velocity of the time-dependent nonlinear equilibrium solution differs from the steady free-stream velocity $f'(\infty) = 1$. For comparison with experimental results it is therefore reasonable to define a new Reynolds number Re_{m} with the new free-stream velocity $u_{\mathrm{m}}(\infty) = 1 + \epsilon_{2\mathrm{D}}\,\hat{u}_0(\infty)$, i.e.

$$Re_{\mathrm{m}} = (x^* u_{\mathrm{m}}^*(\infty)/\nu^*)^{\frac{1}{2}} = Re\,[1 + \epsilon_{2\mathrm{D}}\,\hat{u}_0(\infty)]^{\frac{1}{2}}. \tag{27}$$

As a consequence of $\hat{u}_0(\infty) \leqslant 0$ we have $Re_{\mathrm{m}} \leqslant Re$ and for steady laminar flow (with $\epsilon_{2\mathrm{D}} \equiv 0$) $Re_{\mathrm{m}} = Re$. In engineering applications one uses in general

$$Re_x = x^* u_{\mathrm{m}}^*(\infty)/\nu^* = Re_{\mathrm{m}}^2. \tag{28}$$

A further mean-flow quantity of considerable technical importance is the *local skin-friction factor*

$$c_f' = \frac{\tau_{\mathrm{wall}}^*}{\frac{1}{2}\rho^* u_{\mathrm{m}}^*(\infty)^2}; \tag{29}$$

$\tau_{\mathrm{wall}}^* = \mu^*(\partial u_{\mathrm{m}}^*/\partial y^*)_{y^*=0}$ denotes the wall shear stress and ρ^* is the density. Using our non-dimensionalized quantities we find

$$c_f' = 2\frac{(\partial u_{\mathrm{m}}/\partial y)_{y=0}}{[1+\epsilon_{2\mathrm{D}}\,\hat{u}_0(\infty)]^2\,Re} = 2\frac{Re^3\,(\partial u_{\mathrm{m}}/\partial y)_{y=0}}{Re_{\mathrm{m}}^4}. \tag{30}$$

For the steady Blasius boundary layer with $Re = Re_{\mathrm{m}}$ this reduces to the well-known result

$$c_{f_{\mathrm{lam}}}' = \frac{2(\partial u_{\mathrm{m}}/\partial y)_{y=0}}{Re} = \frac{2f''(0)}{Re}, \quad f''(0) = 0.332\,057. \tag{31}$$

With the prescribed normalization (21) the amplitude $\epsilon_{2\mathrm{D}}$ provides a scalar measure of the nonlinear fluctuations. In theoretical investigations however, instead of $\epsilon_{2\mathrm{D}}$ one generally uses the *total fluctuation energy* E per unit length normalized with $\frac{1}{2}U_\infty^{*2}L^*$:

$$E = \sum_{n=1}^{N} E_n, \quad E_n = \frac{2\epsilon_{2\mathrm{D}}^2}{1+\delta_{n0}}\int_0^\infty [\hat{\boldsymbol{v}}_n(y)\cdot\bar{\hat{\boldsymbol{v}}}_n(y)]\,\mathrm{d}y, \tag{32}$$

with $\hat{\boldsymbol{v}}_n = (\hat{u}_n, \hat{v}_n)$, $\hat{u}_n = \mathrm{d}\hat{\psi}_n/\mathrm{d}y$, $\hat{v}_n = -\mathrm{i}n\alpha\hat{\psi}_n$. Here δ_{n0} denotes Kronecker's delta and a barred quantity is the complex conjugate. In experimental investigations usually *r.m.s. values* are measured, for example the streamwise velocity fluctuation

$$u_{\mathrm{rms}}(y) = \sqrt{2}\,\epsilon_{2\mathrm{D}}\left\{\sum_{n=1}^{N}|\hat{u}_n(y)|^2\right\}^{\frac{1}{2}}. \tag{33}$$

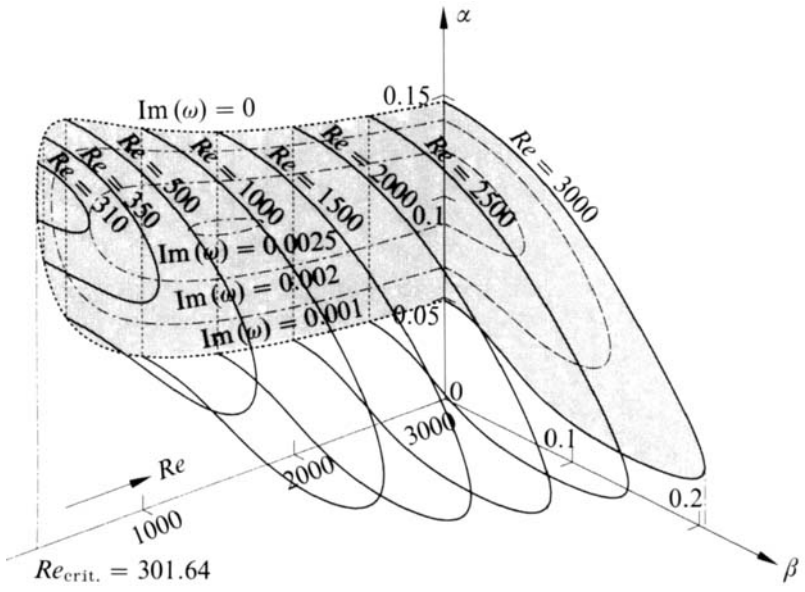

FIGURE 1. Perspective view of three-dimensional linear neutral surface with several temporal amplification curves Im (ω) = constant $(-\cdot-)$ at the bounding cuts.

2.4. *Two-dimensional equilibrium solution*

In order to investigate secondary instabilities we may either employ the shape assumption, cf. Herbert (1988), or compute the exact nonlinear primary equilibrium surface. The shape assumption is a valid approximation near the threshold of secondary instabilities. In our investigation, however, we are also interested in the bifurcation behaviour at higher amplitudes. Therefore we need to compute first the nonlinear primary equilibrium surface. This will be done in the following section.

The starting point of our nonlinear computation is the linear neutral surface depicted in figure 1 for three-dimensional linear waves (β being the spanwise wavenumber). This linear neutral surface describes the location of Hopf bifurcations from the basic laminar state in the parameter space (Re, α, β) and is the result of linear classical hydrodynamic stability theory (cf. Drazin & Reid 1981). Inside the neutral surface the flow is linearly unstable, while outside the surface the flow is linearly stable. Several temporal amplification curves Im (ω) = constant have been inserted for the cuts $\beta = 0$ and $Re = 3000$ in figure 1. The temporal eigenvalue spectrum consists of a finite number of discrete eigenvalues (one of which becomes unstable on the above neutral surface) as well as of a continuous contribution. The critical Reynolds number is reached for two-dimensional disturbances at $Re_{\text{crit}} = 301.64$ with $\alpha_{\text{crit}} = 0.176$, $C_{\text{crit}} = 0.396\,64$ and hence $\omega_{\text{crit}} = \alpha_{\text{crit}} C_{\text{crit}} = 0.0710$ (cf. Drazin & Reid 1981). Consequently the two-dimensional nonlinear equilibrium surface is of greatest interest and we shall limit ourselves in the following to two-dimensional primary disturbances, i.e. $\beta = 0$. On the neutral surface α and ω are both real and there is no distinction between temporal and spatial modes.

A basic question concerns the truncation error of our numerical solution. Truncation influences the quantitative and even qualitative behaviour of the primary neutral surface as well as the secondary instability of §3. As we shall see from a comparison with weakly nonlinear results in §2.5 the historically important mean-field solution with $N = 1$ is even qualitatively incorrect. At higher values of α truncation at $N = 3$ gives fairly accurate results for the primary equilibrium surface

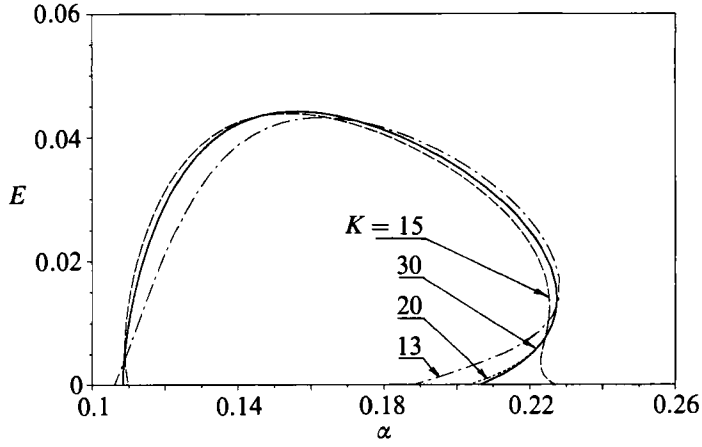

FIGURE 2. Influence of Chebyshev truncation K on the accuracy of fluctuation energy $E(\alpha)$ for $Re = 500$, $N = 1$.

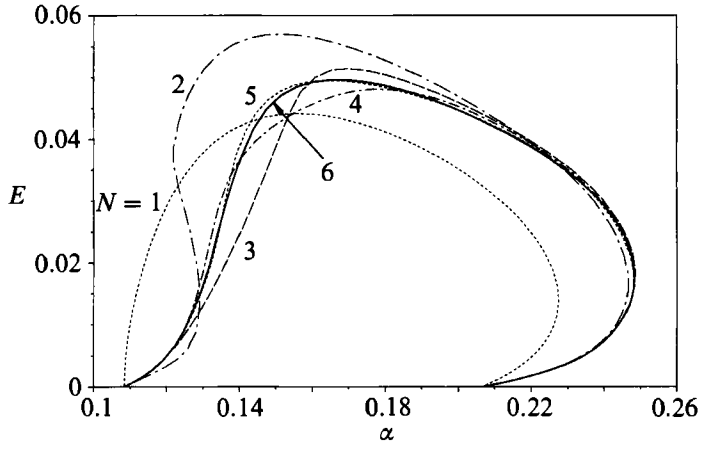

FIGURE 3. Influence of Fourier truncation N on the accuracy of fluctuation energy $E(\alpha)$ for $Re = 500$, $K = 30$.

as well as for the secondary instability computation of §3. It appears fortunate that this high-α part of the neutral surface is also of most importance for our direct resonance analysis, because at low α many more modes need to be retained for quantitatively accurate results. To demonstrate the influence of truncation on the primary equilibrium solution we vary the number of Chebyshev polynomials as well as the number of streamwise Fourier modes. After computing the neutral surface for $N = 1$ and 2 for reference and comparison with the corresponding plane Poiseuille flow results we investigate a single solution in greater detail for the high truncation $N = 6$.

For our truncation test we have chosen the example with fixed Reynolds number $Re = 500$. Keeping at first only one Fourier mode, i.e. $N = 1$, we vary the number of retained Chebyshev polynomials K. Figure 2 demonstrates that for small K the largest deviations occur near the linear neutral curve and that K should be chosen larger than 20. Therefore we fix $K = 30$ in all following computations and vary the number N of retained Fourier modes in figure 3. We notice that even for $N = 6$ the solution has not fully converged quantitatively, but $N = 3$ gives already fairly

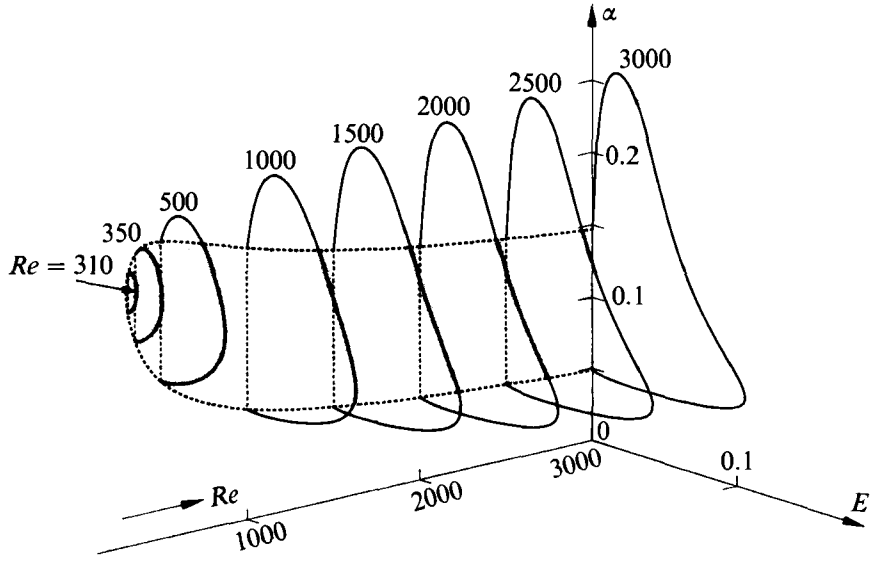

FIGURE 4. Perspective view of two-dimensional neutral fluctuation-energy surface $E(Re, \alpha)$ for $K = 30$, $N = 1$.

accurate results at this Reynolds number. In the following we shall compute several cuts through the neutral surface and study the influence of Fourier truncation N as the Reynolds number Re or streamwise wavenumber α is varied.

First we fix $N = 1$ (frequently termed the mean-field approximation because it only takes into account the interaction between the mean flow and the first harmonic) and use Re as control parameter. A perspective view of the neutral surface $E(\alpha, Re)$ with $N = 1$ is shown in figure 4. With the exception of the supercritical behaviour near the critical Reynolds number the solution is qualitatively similar to that for plane Poiseuille flow, cf. Herbert (1977) or Ehrenstein & Koch (1989). (Here we term a solution *supercritical* in the vicinity of a neutral curve if nonlinear equilibria exist in the linearly unstable parameter domain. Consequently a *subcritical* solution exists in the linearly stable parameter domain only above a certain threshold amplitude.) Using max $|u|$ and the frequency parameter $F = \alpha C/Re$ instead of α, Lifshits & Shtern (1986) have already published the $N = 1$ neutral surface. Owing to their different boundary condition for the mean-flow velocity at infinity we have not performed a quantitative comparison with their results, but the qualitative agreement is apparent. We observe from figure 4 that the $N = 1$ solution is subcritical (with a finite-amplitude threshold) on the upper α-branch in agreement with the results of weakly nonlinear theory. On the lower α-branch however the $N = 1$ solution disagrees with the supercriticality prediction of weakly nonlinear theory (compare §2.5). From figure 3 we see that this is due to the severe truncation at $N = 1$ and we therefore increase our truncation to $N = 2$.

The corresponding neutral surface is depicted in figure 5 by the solid curves. The $N = 2$ solution is now in qualitative agreement with the weakly nonlinear prediction at the lower α-branch. We note that contrary to the $N = 1$ solution of figure 4, the $N = 2$ solution of figure 5 is slightly subcritical with respect to the critical Reynolds number, i.e. we have a finite-amplitude solution at $Re = 300$ while $Re_{\text{crit}} = 301.64$. Deviating from the situation encountered in plane Poiseuille flow (cf. Herbert 1977 or Ehrenstein & Koch 1989), a new phenomenon complicates the picture, which so far has been observed only by Lifshits *et al.* (1989). Namely, aside from the $N = 2$

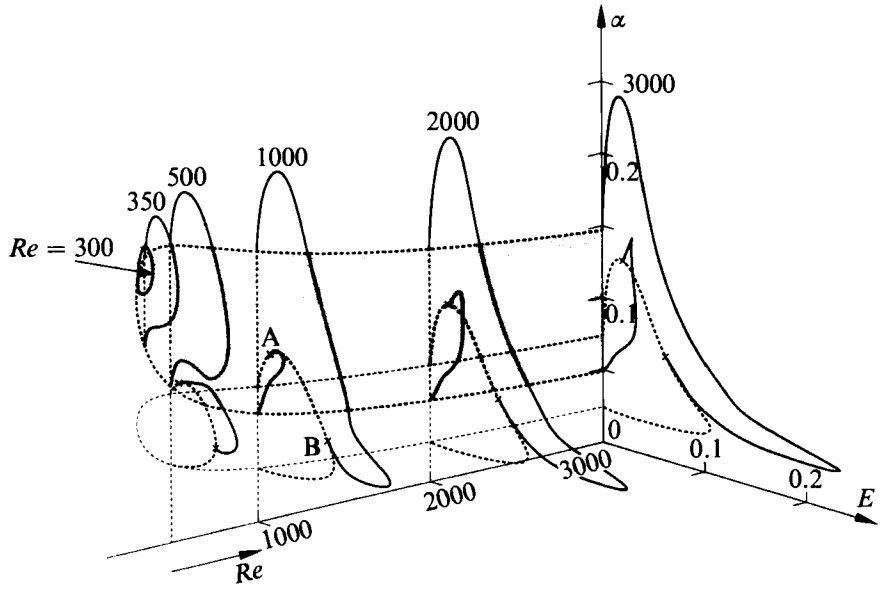

FIGURE 5. Perspective view of two-dimensional neutral fluctuation-energy surface $E(Re, \alpha)$ for $K = 30$, $N = 2$.

branch, shown in figure 3 for $Re = 500$, there exists another $N = 2$ branch which is isolated and originates on the superharmonic neutral surface. (In analogy to a period-doubling *subharmonic* bifurcation with wavenumber α/n, $n = 2$, we term a branch (or bifurcation) *superharmonic* in the streamwise direction if on the bifurcating branch only streamwise harmonics $n\alpha$, $n = 2$ of the original branch with α are excited).

If we increase Re beyond 500 the isolated $N = 2$ branch links up with the $N = 2$ high-α branch and as a consequence the lower branch of the neutral surface can be continued to the upper branch only by including part of the superharmonic neutral surface, for example the section between points A and B for $Re = 1000$ in figure 5. Figure 6(*a*) shows this situation in greater detail for the $N = 2$ solution at $Re = 580$. For $N = 3$ as well as higher truncations we again obtain an isolated finite-amplitude branch at low α. Truncation obviously can change the qualitative behaviour of the solution at lower values of α and we should therefore be very cautious in our interpretation. The isolated $N = 4$ solution (not shown in figure 6*a*) displays an intricate, even more interlooped behaviour and required rather lengthy computations. It is obvious that the isolated $N = 4$ solution has not converged yet and many more modes should be retained which would exhaust our computational resources. Similar remarks apply to the low-α branch at higher Reynolds numbers where even higher truncations lead to a link up of the high-α branch with the superharmonic solution similar to the $N = 2$ solution of figure 6(*a*). However, as we shall see later, the highest local skin friction factor is reached on the high-α portion of the neutral surface where fairly good convergence has already been attained for $N = 3$. Therefore our secondary instability calculations of §3 with $N = 3$ will be still useful if we exclude the low-α part of the two-dimensional equilibrium solution. Figure 6(*b*) displays the corresponding variation of the wave speed C between the linear low- and high-α neutral branch at $Re = 580$ for $N = 1$, 2 and 6. The points where the lower and upper $N = 2$ branches end on the superharmonic neutral surface are marked by crosses in figures 5 and 6. The end points of the isolated $N = 3$ solution

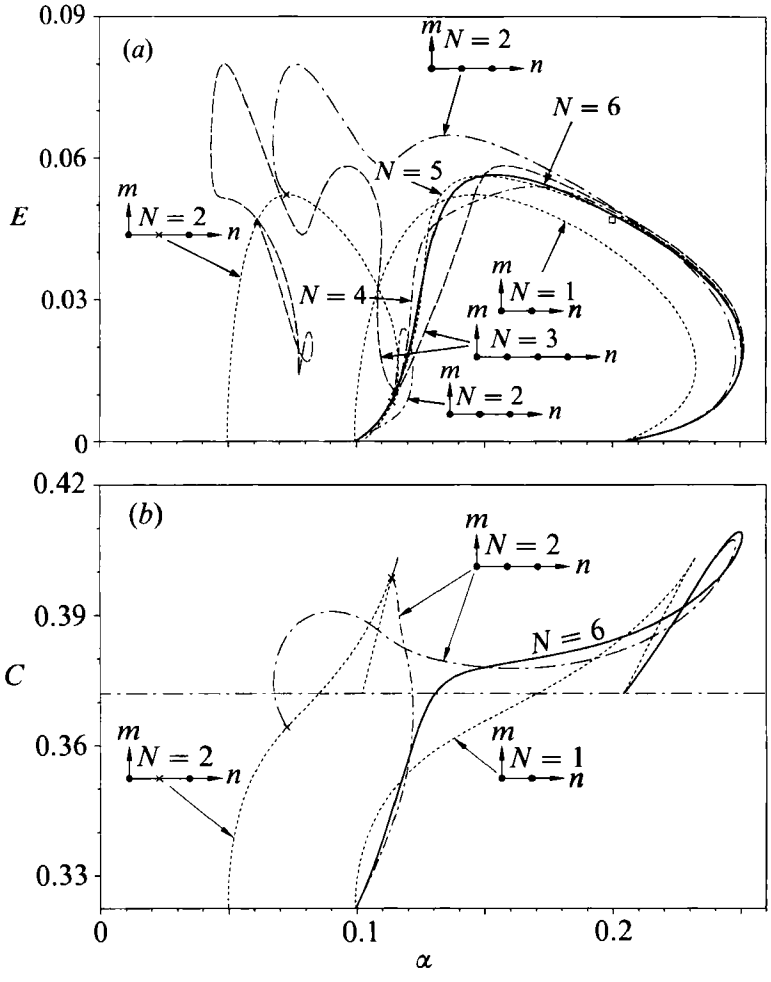

FIGURE 6. (*a*) Influence of Fourier truncation N on the neutral fluctuation-energy surface $E(\alpha)$ for $Re = 580$ with $n = 1, \ldots, 6$. Inserted modal patterns indicate excited modes (●) and non-excited modes (×). The square symbol marks Wagner's equilibrium solution obtained by time-dependent simulation for $\alpha = 0.2$ with $N = 5$. (*b*) Corresponding wave speed $C(\alpha)$ for $Re = 580$ with $N = 1$, 2 and 6.

in figure 6(*a*) are marked by triangles and differ considerably from the crosses of the $N = 2$ solution, a sign of insufficient resolution. These points are interesting examples of a superharmonic 2:1 resonance at finite amplitude.

Taking α as control parameter and varying the Reynolds number we obtain the results depicted in figure 7. Finite-amplitude $N = 2$ resonance points are again marked by crosses. The corresponding superharmonic branches (computed with $N = 1$ and shown as dashed curves) allow a comparison with the $N = 2$ solutions at the same wavenumber α. Obviously more Fourier modes should be retained for quantitatively accurate results. Aside from a factor 2, which might be due to a different definition of E, the results of Milinazzo & Saffman (1985) for $\alpha = 0.17$ lie slightly below our $N = 2$ results. Instead of our Fourier series (5) Milinazzo & Saffman (1985) used a pseudospectral approximation in x and hence their N has a different meaning. But not even with our lowest truncation $N = 1$ did we encounter a spurious bendback as shown in their figure 5 for (their) $N = 7$ truncation. However

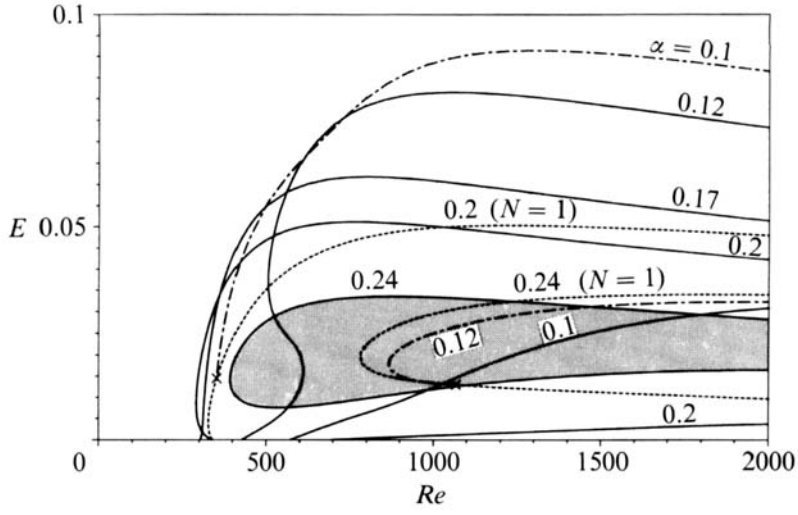

FIGURE 7. Various α = constant cuts through neutral fluctuation-energy surface $E(Re, \alpha)$ for $K = 30$, $N = 2$. Also shown are two cuts for $K = 30$, $N = 1$ (---).

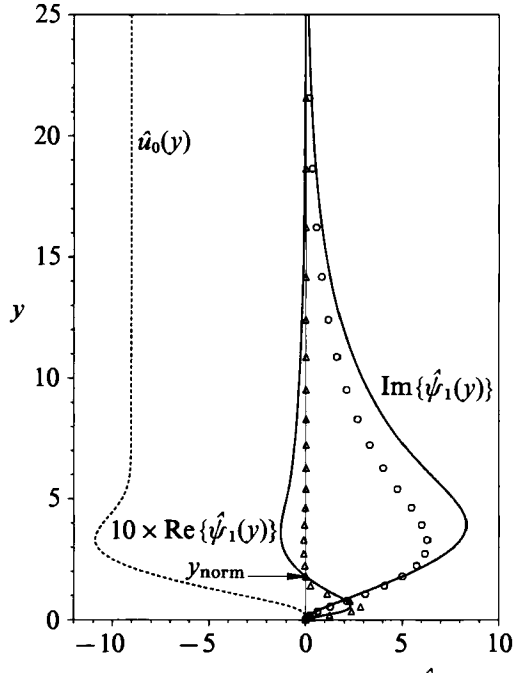

FIGURE 8. Mean-flow distortion $\hat{u}_0(y)$ and fundamental mode $\hat{\psi}_1(y)$ on the large-amplitude branch at $Re = 580$, $\alpha = 0.2$, $C = 0.3842$ with $K = 30$ and $N = 6$ compared with the linear eigenfunction (symbols). Local normalization point is marked by the horizontal arrow.

actual bendbacks are possible as exemplified by the solid line $\alpha = 0.12$ cut in figure 7. It is amazing that the possibility of such a bendback had already been predicted by Likhachev & Shtern (1975) based solely on their weakly nonlinear solution.

An independent check of the nonlinear primary equilibrium solution for $Re = 580$, $\alpha = 0.2$ has been made by M. Wagner at our Institute. Using a modified version of the time-evolution code of Laurien & Kleiser (1989), he obtained the two-dimensional attracting end state $E = 0.046\,89$ with $N = 5$ shown by the square symbol in figure

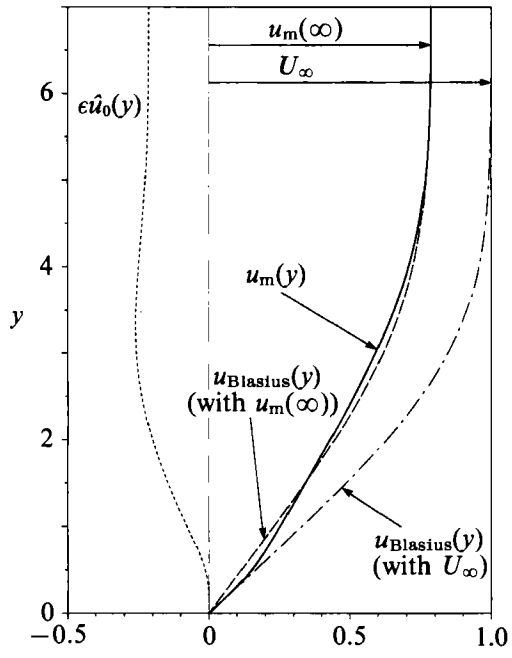

FIGURE 9. Mean-flow velocity $u_m(y) = f'(y) + \epsilon_{2D}\hat{u}_0(y)$ on the large-amplitude branch at $Re = 580$, $\alpha = 0.2$, $C = 0.3842$ with $K = 30$ and $N = 6$. Also shown is the corresponding Blasius profile $f'(y)$ non-dimensionalized with U_∞^* (−·−) and $u_m^*(\infty)$ (−−).

6(*a*). Apparently the upper branch of Blasius boundary-layer flow is stable with respect to two-dimensional disturbances at the above parameters, similar to plane Poiseuille flow (cf. Pugh & Saffman 1988), and the time-periodic end state is reasonably close to our equilibrium value $E = 0.04814$ for $N = 5$. The slight difference might be due to the different formulation of the mean flow boundary condition at infinity: Laurien & Kleiser (1989) use the Dirichlet boundary condition $\hat{u}_0(\infty) \to 0$ while we impose the Neumann boundary condition $d\hat{u}_0/dy(\infty) \to 0$.

To get a better picture of the two-dimensional equilibrium solution at higher amplitudes we investigated the example $Re = 580$, $\alpha = 0.2$ (with $N = 6$, $K = 30$, $Re_m = 514.33$, $\epsilon_{2D} = 0.02367$, $C = 0.3842$, $E = 0.04801$, $c_f' = 0.001852$) in more detail. Figure 8 shows the mean flow deformation $\hat{u}_0(y)$ and the fundamental mode $\hat{\psi}_1(y)$ as a function of normal distance from the plate. We see that the finite free-stream value $\hat{u}_0(\infty) = -9.025$ is reached much faster than $\hat{\psi}_1(\infty) = 0$. The normalization point, where $\hat{v}_1 \equiv -i\alpha\hat{\psi}_1 = 1$, is marked by the horizontal arrow. Using the same normalization, the symbols depicted represent the corresponding linear eigenfunction at the collocation points, giving some clues about the validity of the frequently used shape assumption at higher amplitudes. The mean-flow profile $u_m(y)$ of the nonlinear equilibrium solution is plotted in figure 9 together with the Blasius profiles non-dimensionalized with the original as well as the nonlinearly deformed free-stream velocity. We observe that, with reference to the nonlinearly deformed free-stream velocity, $u_m(y)$ is somehow intermediate between a laminar and a turbulent mean-flow profile. With our constant-pressure-gradient formulation $u_m(y)$ starts with the wall shear stress of the original laminar flow, but ends with the different free-stream velocity $1 + \epsilon_{2D}\hat{u}_0(\infty)$. In the experimentally realized flow the mean-flow profile would end with the free-stream velocity U_∞ but would start with a different wall shear stress.

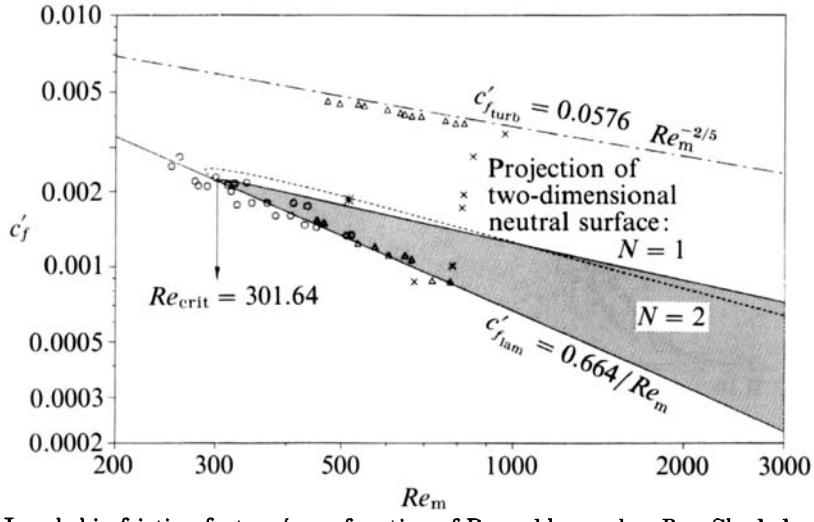

FIGURE 10. Local skin friction factor c_f' as a function of Reynolds number Re_m. Shaded area shows the projection of the $N = 1$ equilibrium surface. Dashed curve indicates projection of $N = 2$ equilibrium surface. Also included are the local skin friction measurements of Dhawan (1953) together with the laminar law of Blasius and the turbulent law of Prandtl (○, direct skin friction measurements at $x^* = 28.6$ cm; △, laminar and turbulent (tripped) direct skin friction measurements at $x^* = 56$ cm; ×, transitional direct skin friction measurements for Mach numbers $M \sim 0.24$ to 0.6). The star marks the location (c_f', Re_m) of our high-amplitude example for $Re = 580$, $\alpha = 0.2$ with $N = 6$.

For engineering applications the skin-friction factor is of major importance. The projection of the local skin friction factor surface $c_f'(Re_m, \alpha)$ is shown in figure 10 for $N = 1$ (shaded area) and $N = 2$, together with Blasius' law $c'_{f_{lam}} = 0.664/Re_m$ for laminar flow and Prandtl's law $c'_{f_{turb}} = 0.057\,6\,Re_m^{-2/5}$ for turbulent flow (cf. Schlichting 1958). The projection of the $N = 2$ neutral surface shows slightly subcritial behaviour with respect to Re_m (see also figure 5) but otherwise deviates only slightly from the projection of the $N = 1$ surface. This situation is similar to that encountered for plane Poiseuille flow, cf. Ehrenstein & Koch (1991), and we assume that the projection of the $N = 2$ neutral surface already gives us a fairly good picture of the projected true surface. This is because the maximal friction factor is almost always located on the high-α branch where good convergence is achieved. The location of maximal friction factor however does not coincide with the location of the maximal fluctuation energy. For comparison the local skin friction measurements of Dhawan (1953) for laminar, turbulent (tripped by a roughness element at the leading edge) and transitional flow on a flat plate are also included. Apparently, in Dhawan's (1953) experiment the transition is quite abrupt and as expected has no relation to the two-dimensional nonlinear equilibrium solution above computed. Transition is a three-dimensional phenomenon and to a certain extent the above two-dimensional equilibrium surface is a mathematical artifice which led to frequent misunderstandings. The saturated high-amplitude equilibrium state is practically never reached in an open-flow system because higher amplified three-dimensional secondary instabilities take over at much lower threshold amplitudes, cf. Herbert (1988) or Lifshits *et al.* (1989). Yet, the primary equilibrium surface is needed for the accurate computation of secondary instabilities unless one uses the approximate shape assumption employed by Herbert (1988).

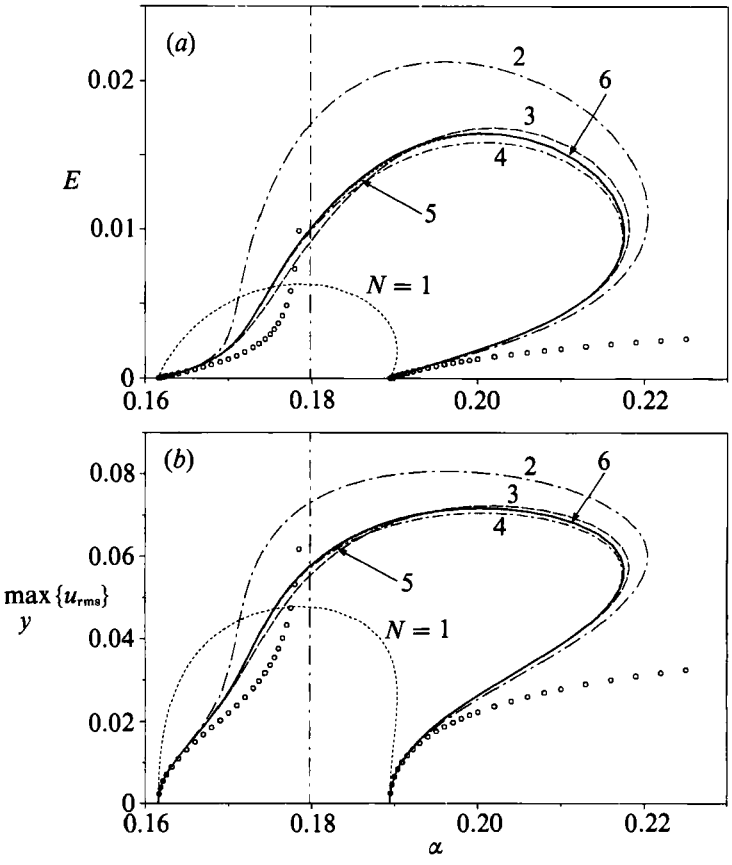

FIGURE 11. Comparison with weakly nonlinear results of Fischer (1990) (○) at $Re = 310$ with $K = 30$ and $N = 1, \ldots, 6$. (*a*) Fluctuation-energy surface $E(\alpha)$, (*b*) maximum r.m.s. value of streamwise velocity fluctuation $\max_{0 \leqslant y < \infty} u_{\mathrm{rms}}(\alpha)$.

2.5. *Comparison with weakly nonlinear results*

The above numerical results give us a welcome chance to assess the range of convergence of weakly nonlinear computations for Blasius flow. Weakly nonlinear amplitude expansions describe the behaviour of the nonlinear solution in the neighbourhood of the linear neutral surface. Despite differing formulations of the various weakly nonlinear theories for Blasius boundary-layer flow (cf. Itoh 1974; Likhachev & Shtern 1975; Herbert 1975; Smith 1979*b*; Sen & Vashist 1989; or Fischer 1990, just to cite a few) the general results are very similar: roughly speaking the solution on the low-α branch is supercritical (Likhachev & Shtern 1975 call it soft excitation) and on the high-α branch it is subcritical (hard excitation). We are especially grateful to Dr T. Fischer at our Institute for providing the relevant weakly nonlinear equilibrium results, which were computed for the same boundary conditions at infinity as ours, cf. Fischer (1990). A more detailed comparison, in particular of the mean flow distortion $\hat{u}_0(y)$ can be found in Fischer (1992).

With $Re = 310$ our Re = constant cut chosen for comparison is near the critical Reynolds number. Figure 11 shows the corresponding results for the fluctuation energy E (figure 11*a*), as well as the maximum streamwise r.m.s. fluctuation $\max_{0 \leqslant y < \infty} u_{\mathrm{rms}}(y)$ (figure 11*b*). We note that even at this very low Reynolds number at least $N = 3$ modes have to be retained in our Fourier expansion to obtain

quantitatively correct results. The higher the Reynolds number the more modes are needed (compare also Conlisk *et al.* 1987). The symbols in figure 11 denote Fischer's weakly nonlinear results near the low- and high-α branch neutral curve, where excellent agreement is found. With increasing amplitudes the deviations increase as expected. Qualitatively the numerical results also agree with Herbert's (1975) weakly nonlinear computation. All together, this comparison not only allows us to assess the range of applicability of weakly nonlinear theory for Blasius flow, but also provides a valuable check on our numerical computation.

2.6. *Connections to high-Reynolds-number theory*

Although outside the main scope of this investigation a very stimulating discussion with F. T. Smith induced us to point out interesting connections between our finite-Reynolds-number results and the high-Reynolds-number solutions of F. T. Smith and his colleagues. High-Reynolds-number theory provides a rational expansion procedure valid in the limit as $Re \to \infty$ and allows a consistent inclusion of non-parallel effects. Strictly valid only for asymptotically large Reynolds numbers it appears to lead to qualitatively and often quantitatively reliable conclusions even for finite Reynolds numbers. Near the lower-wavenumber branch of the neutral curve the weakly nonlinear triple-deck analysis of Smith (1979*b*) shows that nonlinearity is supercritically stabilizing with a (locally) stable limit-cycle solution. The upper branch is subcritically unstable according to Gajjar & Smith (1985) in agreement with our numerical findings, see for example figure 5. Proceeding to higher amplitudes Smith & Burggraf (1985) analysed the development of high-frequency disturbances and were led, *inter alia*, to the Benjamin–Ono equation governing the displacement at high frequencies. This equation allows stable periodic or solitary nonlinear travelling-wave solutions which could possibly be related to our numerical high-amplitude results. In their schematic diagram of the amplitude-dependent neutral curve for asymptotically large Reynolds numbers Smith & Burggraf (1985) or Smith, Doorly & Rothmayer (1990) conjectured a high slope along the lower-wavenumber branch and a low slope with a pronounced bulge on the upper branch which closely resembles our $N = 1$ results of figure 4. The frequency-doubling bifurcation for higher truncations, cf. figure 5, changes this picture drastically unless the solution breakdown of Smith (1988) can be related to this bifurcation. Perhaps this could offer a theoretical explanation for the highly oscillatory behaviour of our numerical solution for low wavenumbers. But, as mentioned before, three-dimensional secondary bifurcations are physically more significant and therefore extensions of the high-Reynolds-number theory to include three-dimensionality are extremely important. In this context it is perhaps worth pointing out that often two-dimensional nonlinear theory is found to apply also to three-dimensional solutions in a locally quasi-two-dimensional manner.

3. Three-dimensional secondary instability

The recognition that the rapid growth of three-dimensional disturbances in transitional boundary-layer flow is due to a linear secondary instability of the two-dimensional finite-amplitude Tollmien–Schlichting waves constituted an important breakthrough in transition research. Floquet theory provides the theoretical tool for classifying and computing the various parametric instabilities as outlined very clearly in Herbert's (1988) review. Yet, similar to primary stability theory, it is not possible to predict transition with secondary stability theory, unless it is

supplemented, usually by empirical information. As Morkovin (1991) formulated it, some additional spontaneous change may yet be needed to explain the rather abrupt changes at transition.

In this section we investigate three-dimensional secondary disturbances of the periodic two-dimensional equilibrium solution computed in §2. Concentrating on so-called fundamental parametric resonances corresponding to phase-locked Klebanoff-type secondary instabilities, cf. Herbert (1988), we identify a modal degeneracy between amplified modes. The associated algebraic growth induced us to speculate whether this direct resonance is possibly one of the spontaneous changes conjectured by Morkovin (1991).

3.1. *Governing equations*

In a frame of reference moving with the velocity C of the two-dimensional nonlinear equilibrium solution we split the dimensionless velocity vector $\boldsymbol{v} \equiv (u, v, w)$ as well as the vorticity vector $\boldsymbol{\omega} \equiv (\xi, \eta, \zeta) = \boldsymbol{\nabla} \times \boldsymbol{v}$ in the usual way into a streamwise-periodic steady base flow plus a time-dependent disturbance:

$$\boldsymbol{v}(x, y, z, t) = [U(y)\,\boldsymbol{i} + \epsilon_{2D}\,\tilde{\boldsymbol{v}}_{2D}(x, y)] + \epsilon\tilde{\boldsymbol{v}}(x, y, z, t), \tag{34a}$$

$$\boldsymbol{\omega}(x, y, z, t) = [-\mathrm{d}U/\mathrm{d}y + \epsilon_{2D}\,\tilde{\xi}_{2D}(x, y)]\,\boldsymbol{k} + \epsilon\tilde{\boldsymbol{\omega}}(x, y, z, t). \tag{34b}$$

Here the bracketed term represents the two-dimensional equilibrium flow computed in §2 with $\boldsymbol{i}$ and $\boldsymbol{k}$ being unit vectors in the x- and z-directions. ϵ denotes the (small) amplitude of the three-dimensional disturbances $\tilde{\boldsymbol{v}}$, $\tilde{\boldsymbol{\omega}}$. There is no need for the shape assumption employed by Herbert (1988), but the parallel-flow approximation is still limiting our approach.

Substituting the definitions (34) into the equations of motion and linearizing for $\epsilon \ll 1$ we obtain the linear secondary-instability equations in the normal velocity ($\tilde{v}$) – normal vorticity ($\tilde{\eta}$) formulation (see Benney & Gustavsson 1981 or Ehrenstein & Koch 1989):

$$\begin{aligned}\left\{\frac{\partial}{\partial t} + (U-C)\frac{\partial}{\partial x} - \frac{1}{Re}\nabla^2\right\}\nabla^2\tilde{v} - \frac{d^2U}{dy^2}\frac{\partial\tilde{v}}{\partial x} + \epsilon_{2D}\Bigg\{\tilde{u}_{2D}\frac{\partial}{\partial x}\nabla^2\tilde{v} + \frac{\partial\tilde{v}_{2D}}{\partial x}\frac{\partial\tilde{\eta}}{\partial z} + \tilde{v}_{2D}\frac{\partial}{\partial y}\nabla^2\tilde{v} \\ + \frac{\partial\tilde{u}_{2D}}{\partial x}\left[\frac{\partial^2\tilde{v}}{\partial x^2} - \frac{\partial^2\tilde{v}}{\partial z^2} - \frac{\partial^2\tilde{v}}{\partial y^2} - 2\frac{\partial^2\tilde{u}}{\partial x\,\partial y}\right] + \frac{\partial\tilde{\xi}_{2D}}{\partial x}\left[\frac{\partial\tilde{v}}{\partial y} + 2\frac{\partial\tilde{u}}{\partial x}\right] \\ + \frac{\partial^2\tilde{\xi}_{2D}}{\partial x^2}\tilde{u} + \frac{\partial\tilde{\xi}_{2D}}{\partial y}\frac{\partial\tilde{v}}{\partial x} + \frac{\partial^2\tilde{\xi}_{2D}}{\partial x\,\partial y}\tilde{v} + \frac{\partial\tilde{v}_{2D}}{\partial x}\left[\frac{\partial^2\tilde{v}}{\partial x\,\partial y} - \frac{\partial^2\tilde{u}}{\partial y^2}\right]\Bigg\} = 0, \end{aligned} \tag{35a}$$

$$\begin{aligned}\left\{\frac{\partial}{\partial t} + (U-C)\frac{\partial}{\partial x} - \frac{1}{Re}\nabla^2\right\}\tilde{\eta} + \frac{\mathrm{d}U}{\mathrm{d}y}\frac{\partial\tilde{v}}{\partial z} \\ + \epsilon_{2D}\left\{\tilde{u}_{2D}\frac{\partial\tilde{\eta}}{\partial x} + \tilde{v}_{2D}\frac{\partial\tilde{\eta}}{\partial y} - \tilde{\xi}\frac{\partial\tilde{v}_{2D}}{\partial x} - \tilde{\eta}\frac{\partial\tilde{v}_{2D}}{\partial y} - \tilde{\zeta}_{2D}\frac{\partial\tilde{v}}{\partial z}\right\} = 0. \end{aligned} \tag{35b}$$

The corresponding solution is subject to the no-slip boundary conditions on the plate $\tilde{v}(y=0) = \partial\tilde{v}/\partial y(y=0) = \tilde{\eta}(y=0) = 0$ and vanishingly small disturbances at $y = \infty$. The continuity equation $\boldsymbol{\nabla}\cdot\tilde{\boldsymbol{v}} = 0$ together with the definition of vorticity $\tilde{\boldsymbol{\omega}} = \boldsymbol{\nabla}\times\tilde{\boldsymbol{v}}$ complete the system of governing equations.

The coefficients of these equations depend on the two-dimensional equilibrium flow and therefore are periodic in the streamwise direction x with period $\lambda_x = 2\pi/\alpha$; but they are independent of z and t. Therefore, using the normal-mode concept in z and

t and applying Floquet theory, we may write for the solution in the moving frame, cf. Herbert (1988)

$$\begin{Bmatrix} \tilde{v}(x,y,z,t) \\ \tilde{\omega}(x,y,z,t) \end{Bmatrix} = \mathrm{e}^{\sigma t}\,\mathrm{e}^{\mathrm{i}\beta z}\,\mathrm{e}^{\gamma x} \sum_{n=-\infty}^{\infty} \begin{Bmatrix} \tilde{v}_n(y) \\ \tilde{\omega}_n(y) \end{Bmatrix} \mathrm{e}^{\mathrm{i}n\alpha x}, \tag{36}$$

with $0 \leqslant \gamma < \alpha$. In our temporal approach σ is a complex quantity with $\mathrm{Re}(\sigma)$ giving the temporal growth rate and $\mathrm{Im}(\sigma)$ being the frequency shift with respect to the two-dimensional equilibrium flow. We are mainly interested in phase-locked disturbances of the Klebanoff-type which travel synchronously with the two-dimensional base flow such that $\mathrm{Im}(\sigma) = 0$ and $\gamma = 0$.

Substituting (36) into (35) together with the spectral representation

$$(\hat{u}_{2\mathrm{D}_n}, \hat{v}_{2\mathrm{D}_n}) = (\mathrm{d}\hat{\psi}_n/\mathrm{d}y,\ -\mathrm{i}n\alpha\hat{\psi}_n)$$

of our equilibrium solution of §2 we obtain the modal equations

$$\left\{\frac{1}{Re}\mathrm{D}^2_{n,1} - \mathrm{i}n\alpha(U-C)\,\mathrm{D}_{n,1} + \mathrm{i}n\alpha\frac{\mathrm{d}^2U}{\mathrm{d}y^2} - \sigma\mathrm{D}_{n,1}\right\}\hat{v}_n - \epsilon_{2\mathrm{D}}\sum_{\nu=-\infty}^{\infty} S^{\mathrm{OS}}_{n-\nu,\nu} = 0, \tag{37a}$$

$$\left\{\frac{1}{Re}\mathrm{D}_{n,1} - \mathrm{i}n\alpha(U-C) - \sigma\right\}\hat{\eta}_n - \mathrm{i}\beta\frac{\mathrm{d}U}{\mathrm{d}y}\hat{v}_n - \epsilon_{2\mathrm{D}}\sum_{\nu=-\infty}^{\infty} S^{\mathrm{SQ}}_{n-\nu,\nu} = 0, \tag{37b}$$

where $\mathrm{D}_{n,m} = \mathrm{d}^2/\mathrm{d}y^2 - k^2_{n,m}$ with $k^2_{n,m} = (n\alpha)^2 + (m\beta)^2$. Using the continuity equation and the definition of vorticity we obtain the following relations:

$$\hat{u}_n = -\frac{\mathrm{i}\{\beta\hat{\eta}_n - n\alpha\mathrm{d}\hat{v}_n/\mathrm{d}y\}}{k^2_{n,1}}, \quad \hat{w}_n = \frac{\mathrm{i}\{n\alpha\hat{\eta}_n + \beta\mathrm{d}\hat{v}_n/\mathrm{d}y\}}{k^2_{n,1}}, \tag{38a, b}$$

$$\hat{\xi}_n = \frac{\mathrm{i}\{n\alpha\mathrm{d}\hat{\eta}_n/\mathrm{d}y + \beta\mathrm{d}^2\hat{v}_n/\mathrm{d}y^2\}}{k^2_{n,1}} - \mathrm{i}\beta\hat{v}_n, \quad \hat{\zeta}_n = \frac{\mathrm{i}\{\beta\mathrm{d}\hat{\eta}_n/\mathrm{d}y - n\alpha\mathrm{d}^2\hat{v}_n/\mathrm{d}y\}}{k^2_{n,1}} + \mathrm{i}n\alpha\hat{v}_n. \tag{38c, d}$$

The convolution terms are then

$$S^{\mathrm{OS}}_{\mu,\nu} = A^{\mathrm{OS}}_{\mu\nu}\hat{v}_\mu + B^{\mathrm{OS}}_{\mu\nu}\frac{\mathrm{d}\hat{v}_\mu}{\mathrm{d}y} + C^{\mathrm{OS}}_{\mu\nu}\frac{\mathrm{d}^2\hat{v}_\mu}{\mathrm{d}y^2} + D^{\mathrm{OS}}_{\mu\nu}\frac{\mathrm{d}^3\hat{v}_\mu}{\mathrm{d}y^3} + E^{\mathrm{OS}}_{\mu\nu}\hat{\eta}_\mu + F^{\mathrm{OS}}_{\mu\nu}\frac{\mathrm{d}\hat{\eta}_\mu}{\mathrm{d}y} + G^{\mathrm{OS}}_{\mu\nu}\frac{\mathrm{d}^2\hat{\eta}_\mu}{\mathrm{d}y^2}, \tag{39a}$$

$$S^{\mathrm{SQ}}_{\mu,\nu} = A^{\mathrm{SQ}}_{\mu\nu}\hat{\eta}_\mu + B^{\mathrm{SQ}}_{\mu\nu}\hat{v}_\mu + C^{\mathrm{SQ}}_{\mu\nu}\frac{\mathrm{d}\hat{\eta}_\mu}{\mathrm{d}y} + D^{\mathrm{SQ}}_{\mu\nu}\frac{\mathrm{d}^2\hat{v}_\mu}{\mathrm{d}y^2}, \tag{39b}$$

with

$$A^{\mathrm{OS}}_{\mu\nu} = -\mathrm{i}\alpha\left[n\frac{\mathrm{d}^3\hat{\psi}_\nu}{\mathrm{d}y^3} + (\mu-\nu)\,k^2_{n,1}\frac{\mathrm{d}\hat{\psi}_\nu}{\mathrm{d}y}\right], \tag{40a}$$

$$B^{\mathrm{OS}}_{\mu\nu} = \mathrm{i}\nu\alpha\left\{-\frac{\mathrm{d}^2\hat{\psi}_\nu}{\mathrm{d}y^2}\left(\frac{\beta^2 - \mu n\alpha^2}{k^2_{\mu,1}}\right) + \hat{\psi}_\nu k^2_{n,1}(1 - \nu\mu\alpha^2/k^2_{\mu,1})\right\}, \tag{40b}$$

$$C^{\mathrm{OS}}_{\mu\nu} = \mathrm{i}\alpha\frac{\mathrm{d}\hat{\psi}_\nu}{\mathrm{d}y}(n - 2\nu\beta^2/k^2_{\mu,1}), \quad D^{\mathrm{OS}}_{\mu\nu} = -\mathrm{i}\nu\alpha\hat{\psi}_\nu(1 + \nu\mu\alpha^2/k^2_{\mu,1}), \tag{40 c, d}$$

$$E^{\mathrm{OS}}_{\mu\nu} = \mathrm{i}\nu\alpha^2\beta\{\nu k^2_{n,1}\hat{\psi}_\nu - (2\mu+\nu)\,\mathrm{d}^2\hat{\psi}_\nu/\mathrm{d}y^2\}/k^2_{\mu,1} \tag{40e}$$

$$F^{\mathrm{OS}}_{\mu\nu} = -\frac{\mathrm{i}2\nu\mu\beta\alpha^2}{k^2_{\mu,1}}\frac{\mathrm{d}\hat{\psi}_\nu}{\mathrm{d}y}, \quad G^{\mathrm{OS}}_{\mu\nu} = \mathrm{i}\nu^2\alpha^2\beta\hat{\psi}_\nu/k^2_{\mu,1} \tag{40f, g}$$

$$A^{\mathrm{SQ}}_{\mu\nu} = \mathrm{i}n\alpha\,\mathrm{d}\hat{\psi}_\nu/\mathrm{d}y, \quad B^{\mathrm{SQ}}_{\mu\nu} = \mathrm{i}\beta\,\mathrm{d}^2\hat{\psi}_\nu/\mathrm{d}y^2, \tag{41 a, b}$$

$$C^{\mathrm{SQ}}_{\mu\nu} = -\mathrm{i}\nu\hat{\psi}_\nu\{1 + \nu\mu\alpha^2/k^2_{\mu,1}\}, \quad D^{\mathrm{SQ}}_{\mu\nu} = -\mathrm{i}(\nu\alpha)^2\beta\hat{\psi}_\nu/k^2_{\mu,1}. \tag{41 c, d}$$

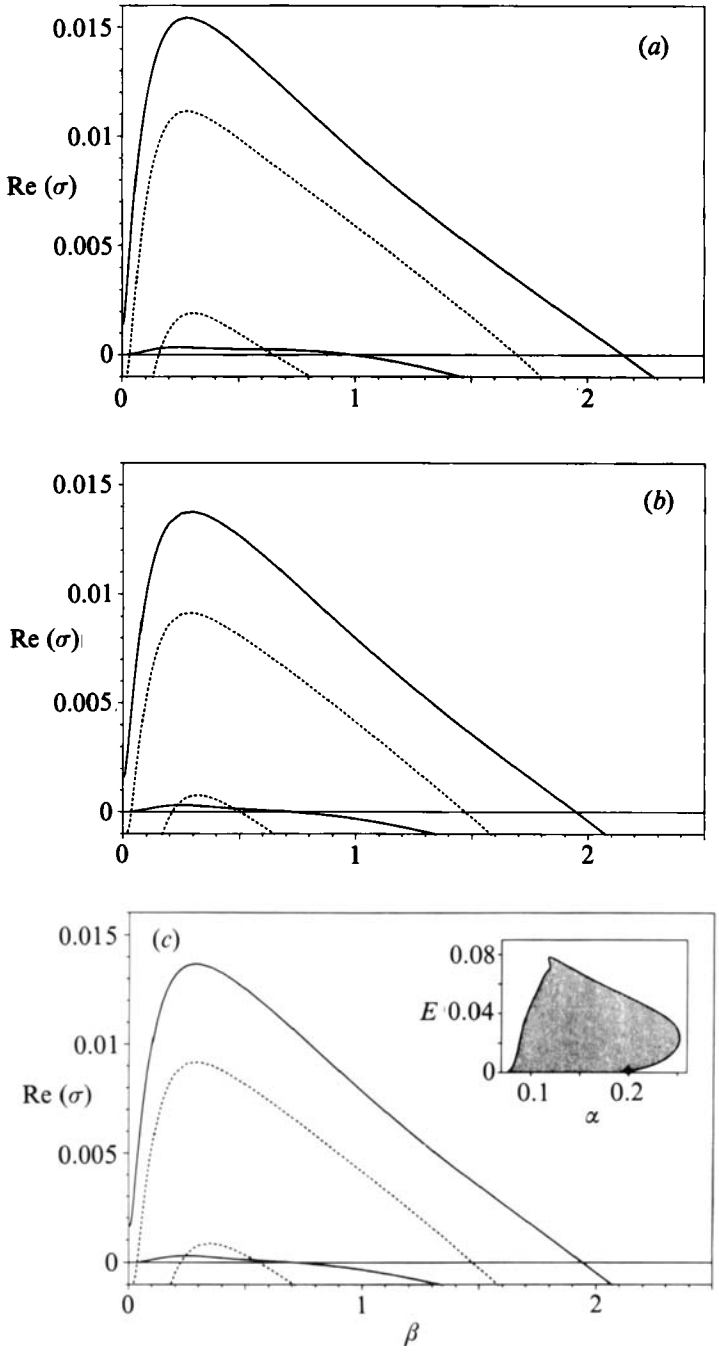

FIGURE 12. Growth rate $\mathrm{Re}(\sigma)$ of phase-locked (—) and non-phase-locked (----) secondary instability modes as function of spanwise wavenumber β for the low-amplitude equilibrium solution at $Re = 1000$, $\alpha = 0.2$ with $K = 30$ and (*a*) $N = 1$, (*b*) $N = 2$ and (*c*) $N = 3$. The point in the insert of figure (*c*) marks the position of the equilibrium solution on the two-dimensional neutral surface for $N = 3$.

For the numerical treatment the secondary instability eigenvalue problem (37) is truncated at $-N \leqslant n \leqslant N$. After applying the exponential mapping of §2, Chebyshev collocation is used to discretize the system of ordinary differential equations (37) as for the two-dimensional equilibrium problem of §2. The ensuing algebraic eigenvalue problem can then be solved by means of standard eigenvalue routines.

3.2. *Three-dimensional secondary instability results and modal degeneracy*

Similar to our truncation discussion in §2.4 we test the accuracy of the secondary instability results by varying the truncation N. In order to demonstrate the influence of the primary instability amplitude we perform this computation for a low- and a high-amplitude example. At the low amplitude, corresponding to the threshold amplitude of secondary instabilities, the shape assumption is clearly good enough and truncation at $N = 2$ appears to be sufficient. At the high amplitude $N = 3$ truncation gives quantitatively adequate results for the most unstable mode. However, qualitative changes are still possible for the higher-order modes at high amplitudes. Nevertheless, truncation at $N = 3$ seems good enough to demonstrate a modal degeneracy at lower amplitudes with possibly far-reaching physical implications.

To investigate the influence of Fourier truncation N on the secondary instability results we fix at first $Re = 1000$, $\alpha = 0.2$ and retain $K = 30$ Chebyshev polynomials in $(0, 1]$ for all computations. Figure 12 shows the corresponding temporal growth rates of the secondary instability modes on the *low-amplitude* equilibrium branch as a function of spanwise wavenumber β for $N = 1, 2$ and 3 (the position on the $N = 3$ equilibrium surface is marked by the point in the insert of figure 12*c*). The solid curves represent phase-locked fundamental modes with $\mathrm{Im}(\sigma) = 0$ while the dashed curves mark non-phase-locked modes which we shall disregard in this study. We note that there is almost no difference between the results for $N = 1$ and $N = 3$ at this very low equilibrium amplitude. Yet the secondary amplification rates are already considerable, confirming the statement that these three-dimensional disturbances are physically more important than the superharmonic two-dimensional solutions found in §2.

The situation changes drastically if we consider the *high-amplitude* equilibrium branch, cf. figure 13. We note that several amplified phase-locked modes exist. While the most unstable mode seems to be fairly accurate for $N = 3$ (only minor changes exist between the $N = 2$ and $N = 3$ results) there are still qualitative changes for the higher-order modes, indicating that more Fourier modes should be retained. Again the solid curves represent phase-locked modes while the dotted curves typify non-phase-locked modes (not included in figure 13*c*). Nevertheless, whatever the accuracy of the $N = 3$ results of figure 13(*c*) is, it is apparent that some of the amplified higher-order modes are near coalescence. This immediately gives rise to the question whether such a modal coalescence could occur between the most-amplified and a higher-order mode. In our problem we have two more parameters that we can vary, namely Re and α. Keeping $Re = 1000$ still fixed we vary α on the two-dimensional equilibrium surface between the low- and high-amplitude point at $\alpha = 0.2$. The resulting phase-locked modes for $N = 3$ are shown in figure 14 (the corresponding position on the two-dimensional equilibrium surface is marked in the inserts of figure 14).

Starting with $\alpha = 0.24$ on the low-amplitude branch (figure 14*a*) we note that for fixed β the various amplified phase-locked modes can be classified, as customary, in descending order of their rate of growth. Only in the damped region does there

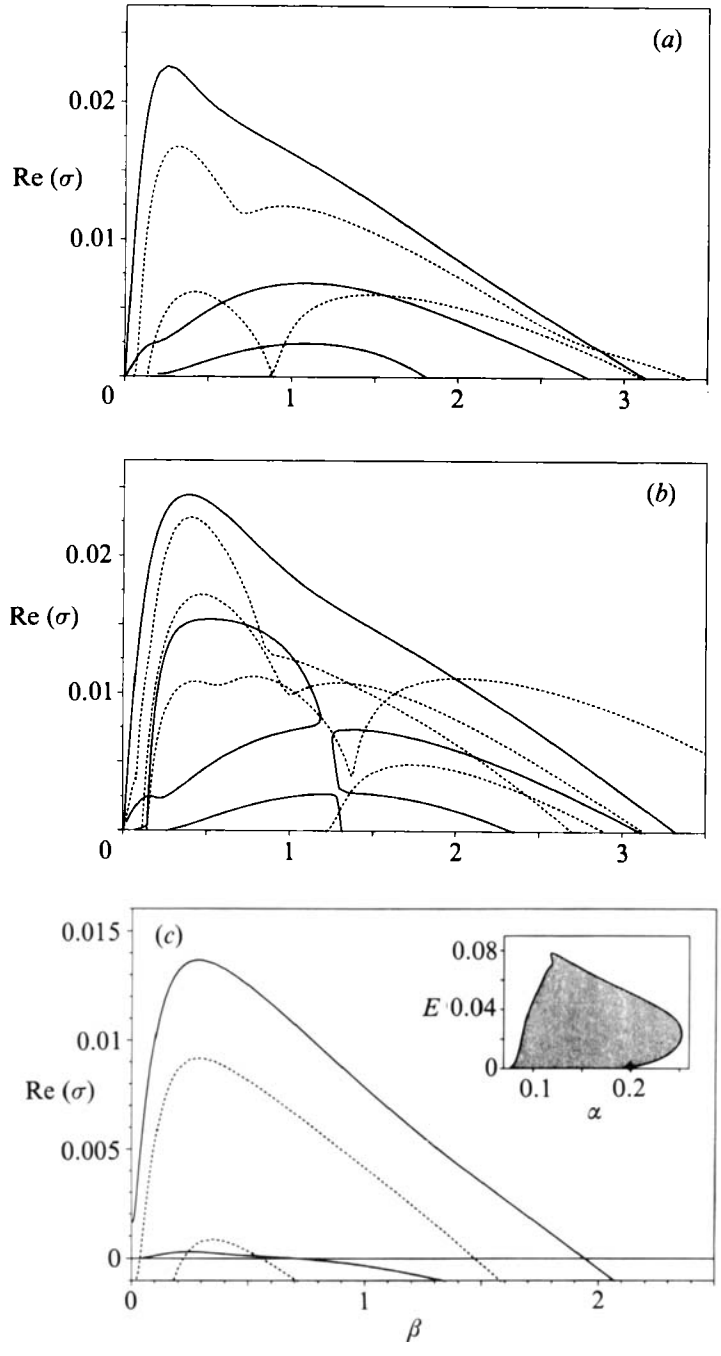

FIGURE 13. Growth rate $\mathrm{Re}(\sigma)$ of phase-locked (—) and non-phase-locked (----) secondary instability modes as a function of spanwise wavenumber β for the high-amplitude equilibrium solution at $Re = 1000$, $\alpha = 0.2$ (marked in the insert on c) with $K = 30$ and (a) $N = 1$, (b) $N = 2$ and (c) $N = 3$.

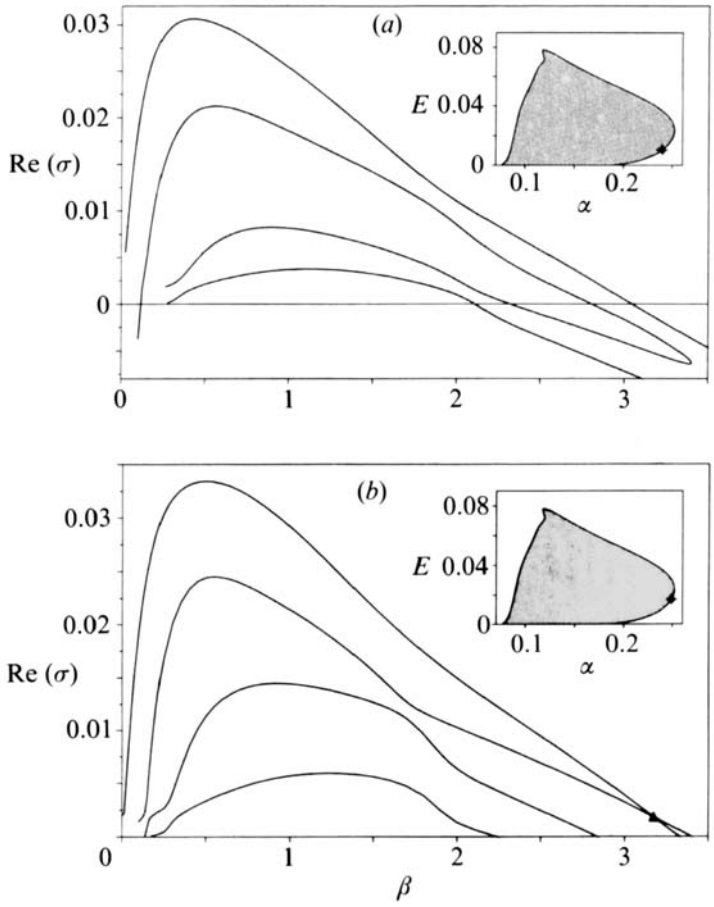

FIGURE 14 (*a*, *b*). For caption see facing page.

already exist a link between the second and third mode. Around $\alpha = 0.24952$ (figure 14*b*) we observe a coalescence between the first and second modes near $\beta \approx 3.17$. What makes this degeneracy even more exciting is the fact that it occurs in the amplified regime. All hitherto known degeneracies between primary instability modes, cf. for example Benney & Gustavsson (1981), Gustavsson (1986), Koch (1986), Jones (1988) or Shantini (1989), are in the damped regime. Increasing the two-dimensional equilibrium amplitude further we find the results shown in figure 14(*c*) for $\alpha = 0.25$. (The usual first- and second-order phase-locked modes do not exist in a finite-β range where the third mode becomes the least damped phase-locked mode. In this finite-β range, where the first and second phase-locked modes cease to exist, a complex-conjugate pair of non-phase-locked modes occurs along the dashed line shown in figure 14(*c*). This means that in the moving system a time-periodic solution appears, which corresponds to a two-frequency solution in the laboratory-fixed system. However, in our present study we exclude such quasi-periodic solutions). We have already encountered such behaviour in figure 14 of Ehrenstein & Koch (1991) where this was the reason for the rather unusual lobed form of the neutral secondary amplification curve. In Ehrenstein & Koch (1991) we used the approximate quasi-equilibrium approach of Orszag & Patera (1983) while here we employ the 'exact' two-dimensional equilibrium solution without shape assumption which is 'exact' to within the parallel-flow approximation. If we increase the

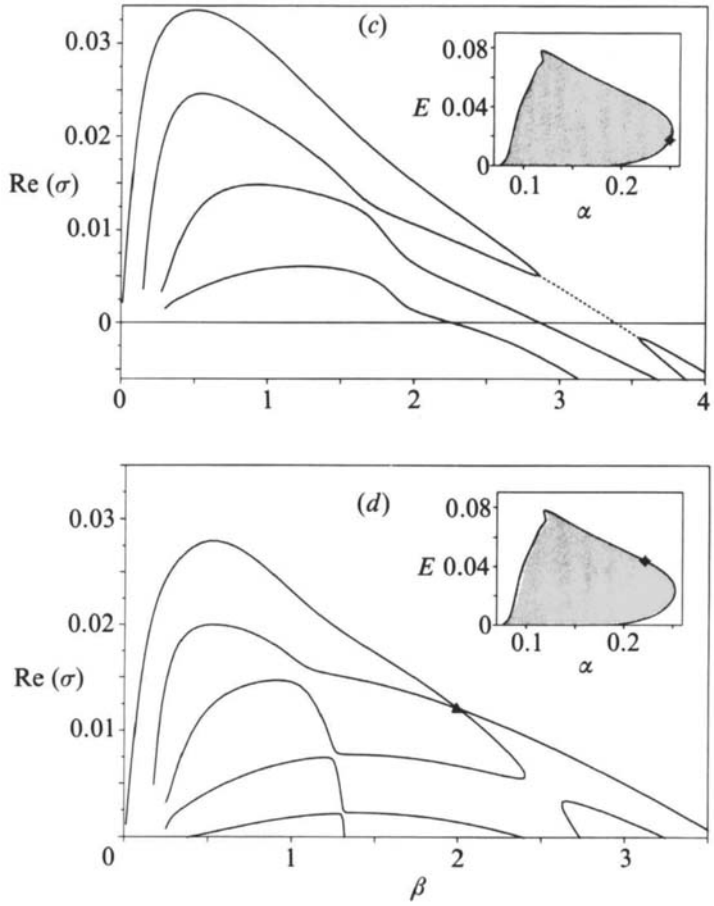

FIGURE 14. Growth rate $\mathrm{Re}(\sigma)$ of phase-locked secondary instability modes as a function of spanwise wavenumber β for $Re = 1000$, $K = 30$, $N = 3$, with (*a*) $\alpha = 0.24$, (*b*) $\alpha = 0.24952$, (*c*) $\alpha = 0.25$ and (*d*) $\alpha = 0.22161$. The points in the inserts mark the corresponding positions of the equilibrium solution on the two-dimensional neutral surface for $N = 3$ and the solid triangles indicate a modal degeneracy.

amplitude further we find another degeneracy of the first mode near $\alpha = 0.22161$, $\beta \approx 1.99$ (cf. figure 14*d*) on the high-amplitude equilibrium surface before we reach the high-amplitude results of figure 13(*c*).

The modal degeneracy above described implies the coincidence of two amplified eigenvalues, i.e. the double eigenvalue has an algebraic multiplicity of two, cf. Iooss & Joseph (1980). The eigenvectors corresponding to this double eigenvalue also coincide, i.e. the geometric multiplicity is one indicating a non-semisimple 1:1 resonance. Generalized eigenvectors have to be introduced and the local amplification rate is $t\exp(\sigma t)$, i.e. algebraic. As a side remark we note that the geometric multiplicity of our bicritical bifurcation points for the plane Poiseuille flow problem in Ehrenstein & Koch (1991) was two and hence they were semisimple because the coinciding eigenvalues belonged to linearly independent families of eigenmodes, i.e. symmetric–antisymmetric, or first and second spanwise harmonic.

The qualitative implications of this algebraic growth are sketched in figure 15. While an exponentially amplified mode needs a certain time to reach a prescribed finite amplitude (depending on its rate of amplification) an algebraically amplified

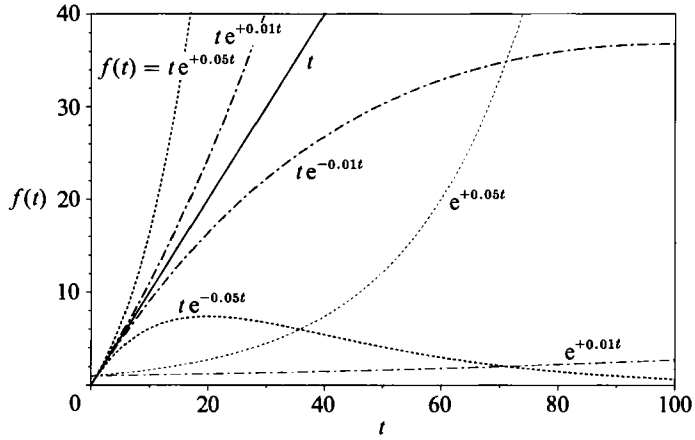

FIGURE. 15. Schematic demonstrating the effect of direct resonance on the temporal amplitude evolution.

mode starts off comparatively abrupt. This is already true for algebraically damped modes. If the damping is weak these modes can reach relatively high amplitudes, possibly initiating nonlinear effects. A neutral or amplified algebraic mode can not only sustain itself linearly but can also lead to explosive changes within a relatively short period of time, making direct resonances a plausible mechanism to occur during transition.

To see how the amplification rate of the low-amplitude point of degeneracy, cf. figure 14(*b*), changes with Reynolds number we vary our last parameter Re. As depicted in figure 16(*a*) there is a fairly clear change from the resonance point being in the amplified region to the resonance point being damped as we decrease Re. The cross-over point is near $Re_{\mathrm{m}} \approx 890$ and corresponds to a double bifurcation point. Figure 17 depicts the growth rates of the phase-locked secondary instability modes for $Re = 910$, $\alpha = 0.232\,92$ (with $Re_{\mathrm{m}} = 887.7$, $Re_x = 7.88 \times 10^5$, $E = 0.006\,75$, $C = 0.387$, $c_f' = 0.806 \times 10^{-3}$) which is reasonably close to this double-bifurcation-point condition. Comparing this with Dhawan's (1953) local skin-friction measurements, reshown in figure 16(*b*) together with the projection of the resonance points on the two-dimensional equilibrium surface (marked by the solid triangles), we observe that the cross-over point lies in the vicinity of the measured increase in local skin friction during transition. Furthermore, $Re_{\mathrm{m}} \approx 890$ also lies very close to the sudden increase in wall shear as computed by Chang *et al.* (1991) for fundamental breakdown at the Mach number $M = 1.6$ using the parabolized stability equations.

From the insert of figure 17 we see that the amplitude E of the two-dimensional disturbance at this double bifurcation point is already substantial. The free-stream turbulence level in Dhawan's (1953) experiment was $u'/U = 0.03\,\%$. On the other side Schubauer & Skramstad (1948), see also Dhawan & Narasimha (1958), found transition at much higher Reynolds numbers, a consequence of different free-stream conditions. If direct resonances were to have anything to do with transition, the amplitude of the two-dimensional disturbance at direct resonance must play a role. Keeping $Re = 910$ constant but following the link-up of the second and third mode, cf. figure 14(*a*), to lower values of α we found a direct resonance between these modes near $\alpha = 0.2182$ as shown in figure 18. This direct resonance occurs in the damped regime, but if we increase the Reynolds number we find that this direct resonance can become amplified near $Re \approx 1900$ ($Re_x \approx 3.6 \times 10^6$) as depicted in figure 19.

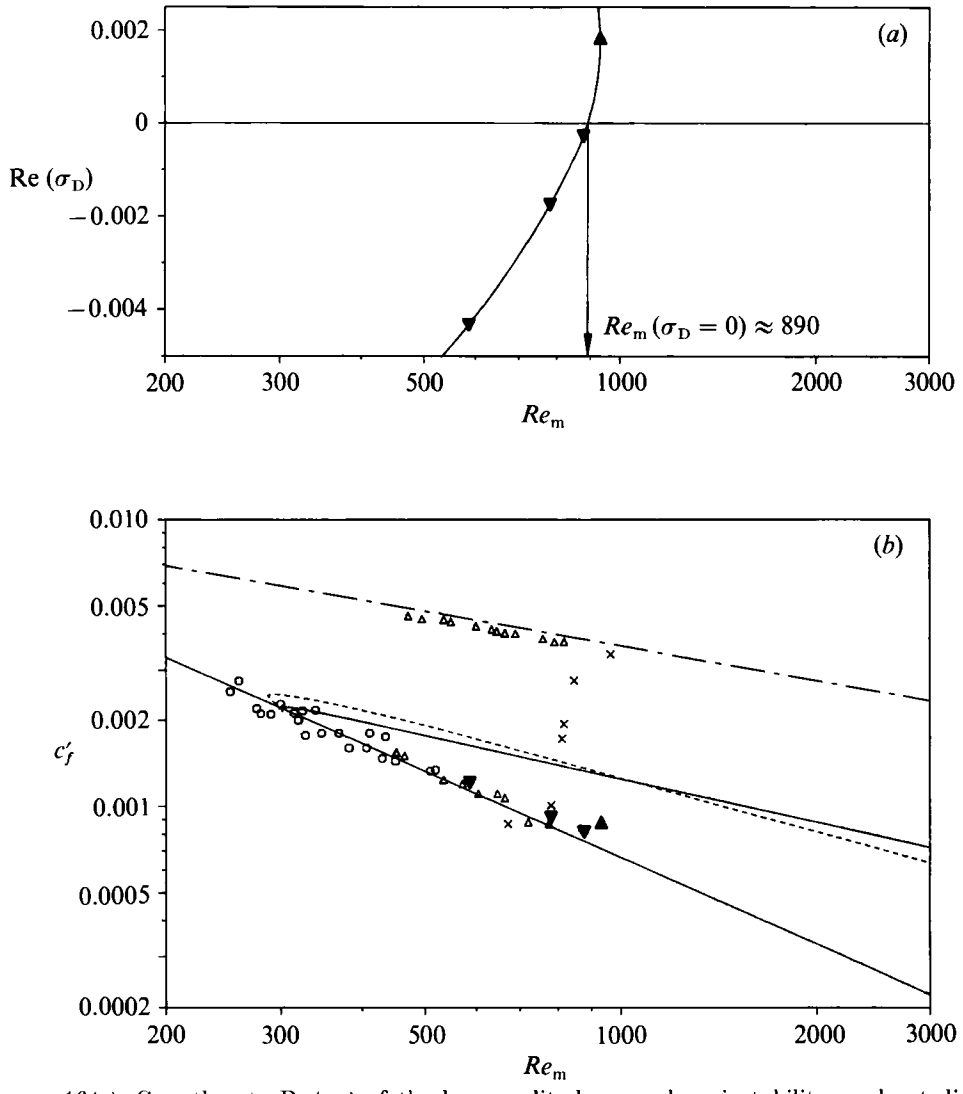

FIGURE 16(*a*). Growth rate $\mathrm{Re}(\sigma_D)$ of the low-amplitude secondary instability mode at direct resonance as a function of Reynolds number Re_m for $K = 30$ and $N = 3$: ▲, amplified direct resonance point; ▼, damped direct resonance point. (*b*) The corresponding location of the direct resonance points on the projected c_f'–Re_m equilibrium surface of figure 10.

Remarkably, this direct resonance between the second and third mode occurs at much lower amplitude E, cf. insert of figure 19, and at a Reynolds number which lies in the vicinity of the e^N-result with $N = 9$. All this might be coincidental. But aside from being of interest in itself, we believe it to be worthwhile to have a closer look at these direct resonances in order to verify or disprove the hypothetical connection with transition.

4. Conclusions

Applying the parallel-flow assumption and using a Fourier expansion in the streamwise direction as well as Chebyshev collocation in the exponentially transformed wall-normal direction, we investigated secondary instabilities in a

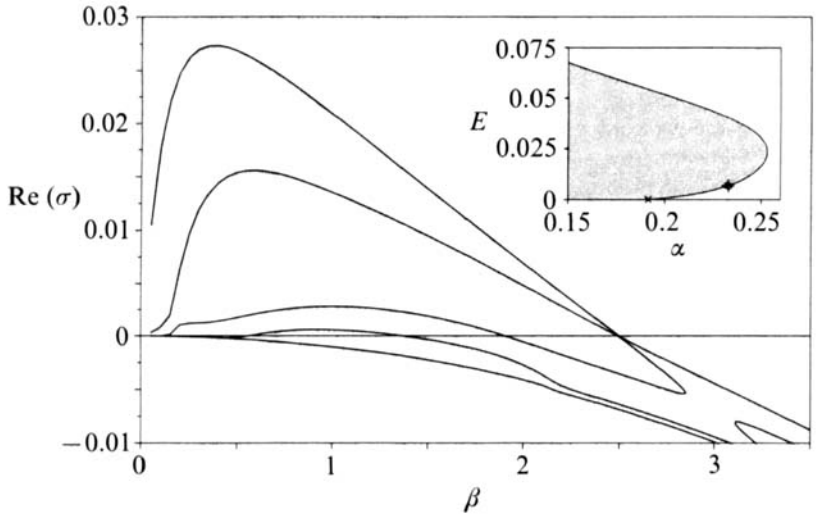

FIGURE 17. Growth rate Re (σ) of phase-locked secondary instability modes as a function of spanwise wavenumber β for $Re = 910$, $\alpha = 0.23292$ with $K = 30$ and $N = 3$.

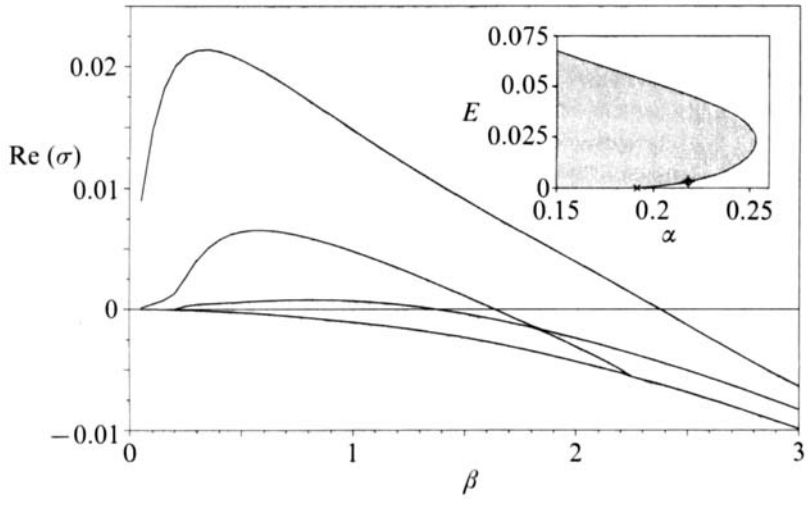

FIGURE 18. Growth rate Re (σ) of phase-locked secondary instability modes as a function of spanwise wavenumber β for $Re = 910$, $\alpha = 0.2182$ with $K = 30$ and $N = 3$.

Blasius boundary layer at finite Reynolds numbers. A first step required the computation of the primary instability neutral surface of two-dimensional nonlinear Tollmien–Schlichting waves. Unlike plane Poiseuille flow, but in agreement with findings of Lifshits *et al.* (1989), two-dimensional superharmonic *period-halving bifurcations* were observed for truncations $N \geqslant 2$. As noted by Lifshits *et al.* (1989) these two-dimensional superharmonic bifurcations occur at large amplitudes and therefore are physically less important than the three-dimensional low-amplitude secondary bifurcations, cf. Herbert (1988).

Using the two-dimensional equilibrium solutions above described as base flow we investigated the stability of this primary equilibrium solution with respect to three-dimensional secondary disturbances in the second part of the paper. Only Klebanoff-type fundamental disturbances are considered which are phase locked to the motion

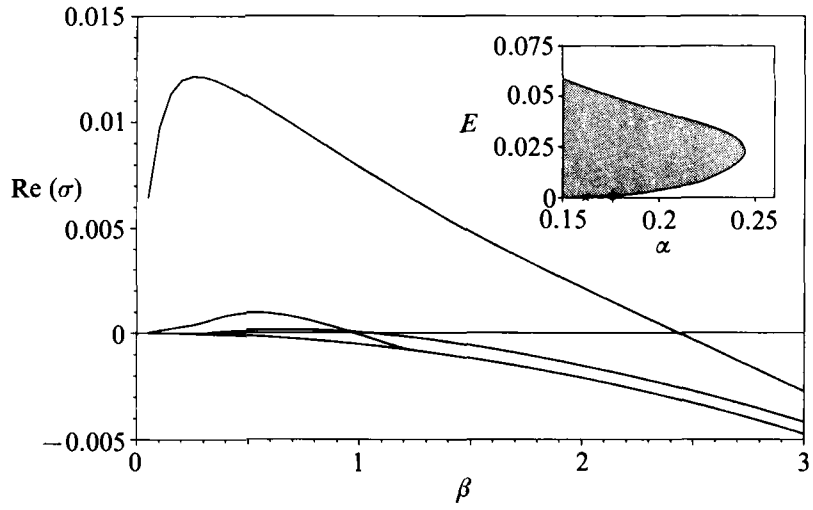

FIGURE 19. Growth rate $\mathrm{Re}(\sigma)$ of phase-locked secondary instability modes as a function of spanwise wavenumber β for $Re = 1900$, $\alpha = 0.176$ with $K = 30$ and $N = 3$.

of the base flow. In addition to the well-known properties of secondary instabilities *modal degeneracies* were detected between amplified secondary instability modes. Frequently termed direct resonances these modal degeneracies indicate locally algebraic growth and constitute the main result of this study. Direct resonances occur at distinct points in the Reynolds number–wavenumber parameter space. Tracing these direct resonances to the point of zero amplification, the corresponding zero-amplification Reynolds number amazingly enough turns out to be in the vicinity of the experimentally observed transition in Blasius flow and one is tempted to link this rather explosive algebraic growth to the abrupt changes observed during transition. However, this agreement might be purely coincidental and before drawing far-reaching conclusions more penetrating studies are necessary to clarify this. In particular, higher modal truncations should be computed to check how much they affect the results quantitatively and the applicability of the parallel-flow assumption has to be assessed. While an experimental test is probably impossible owing to the instability of most of these intermediate equilibrium states, time-dependent numerical simulations might offer a viable alternative. In the mean time more general flows, like Falkner–Skan boundary layers or three-dimensional Falkner–Skan–Cooke flows will be studied to see if this modal degeneracy persists and has the correct trend.

The author is grateful to Dr G. Schneider for making his laminar boundary-layer code available and to Dr T. Fischer for providing the results of his weakly nonlinear theory as well as for valuable discussions concerning the mean-flow boundary condition at infinity. The time-evolution computations of M. Wagner and helpful discussions with Dr U. Ehrenstein concerning the multiplicity of eigenvalues are gratefully acknowledged, as are Professor F. T. Smith's comments on the various connections to high-Reynolds-number theory. The author is indebted to the referees for their constructive criticism and to Dr U. Dallmann for critically reviewing the manuscript. Finally, it is a pleasure to thank Mr L. Leopold for his expert help with the computer plots.

This paper is dedicated to Professor W. R. Sears on the occasion of his 80th birthday.

REFERENCES

BARKLEY, D. 1990 Theory and predictions for finite-amplitude waves in two-dimensional plane Poiseuille flow. *Phys. Fluids* A **2**, 955–970.

BENNEY, D. J. & GUSTAVSSON, L. H. 1981 A new mechanism for linear and nonlinear hydrodynamic instability. *Stud. Appl. Maths* **64**, 185–209.

BERTOLOTTI, F. P. 1991*a* Linear and nonlinear stability of the boundary layers with streamwise varying properties. Ph.D. thesis, The Ohio State University.

BERTOLOTTI, F. P. 1991*b* Compressible boundary layer stability analyzed with the PSE equations. *AIAA Preprint* 91–1637.

BOYD, J. P. 1989 *Chebyshev & Fourier Spectral Methods*. Lecture Notes in Engineering, vol. 49. Springer.

BRIDGES, T. J. 1991 A dynamical systems approach to boundary layer transition. *Warwick Preprint* 2/1991.

CHANG, C.-L., MALIK, M. R., ERLEBACHER, G. & HUSSAINI, M. Y. 1991 Compressible stability of growing boundary layers using parabolized stability equations. *AIAA Preprint* 91-1636.

CLIFFE, K. A. 1988 Numerical calculations of the primary-flow exchange process in the Taylor problem. *J. Fluid Mech.* **197**, 57–79.

CONLISK, A. T., BURGGRAF, O. R. & SMITH, F. T. 1987 Nonlinear neutral modes in the Blasius boundary layer. In *Forum on Unsteady Separation*. ASME FED vol. **52**, pp. 119–121.

DHAWAN, S. 1953 Direct measurements of skin friction. *NACA Rep.* 1121.

DHAWAN, S. & NARASIMHA, R. 1958 Some properties of boundary layer flow during transition from laminar to turbulent flow. *J. Fluid Mech.* **3**, 418–436.

DRAZIN, P. G. & REID, W. H. 1981 *Hydrodynamic Stability*. Cambridge University Press.

ECKHAUS, W. 1965 *Studies in Non-Linear Stability Theory*. Springer.

EHRENSTEIN, U. 1988 Lösung der linearen, inkompressiblen Stördifferentialgleichungen mittels Chebyshev-Kollokation. *Internal DFVLR-Rep.* IB 221–88 A 09.

EHRENSTEIN, U. & KOCH, W. 1989 Nonlinear bifurcation study of plane Poiseuille flow. *DLR Res. Rep.* FB 89–42.

EHRENSTEIN, U. & KOCH, W. 1991 Three-dimensional wave-like equilibrium states in plane Poiseuille flow. *J. Fluid Mech.* **228**, 111–148.

FASEL, H. 1976 Investigation of the stability of boundary layers by a finite-difference model of the Navier–Stokes equations. *J. Fluid Mech.* **78**, 355–383.

FISCHER, T. M. 1990 Ein mathematisch-physikalisches Modell zur Beschreibung transitioneller Grenzschichtströmungen I. Die linearen und nichtlinearen Störungsdifferentialgleichungen. *DLR Res. Rep.* FB 90–24 (with corrigendum).

FISCHER, T. M. 1991 On the nonlinear development of disturbances in boundary layers. *Eur. J. Mech.* B *Fluids* **10** (suppl.), 310).

FISCHER, T. M. 1992 On the nonlinear development of disturbances in boundary layers. *Stud. Appl. Maths.* (submitted).

GAJJAR, J. & SMITH, F. T. 1985 On the global instability of free disturbances with a time-dependent nonlinear viscous critical layer. *J. Fluid Mech.* **157**, 53–77.

GOTTLIEB, D., HUSSAINI, M. Y. & ORSZAG, S. A. 1984 Theory and applications of spectral methods. In *Spectral Methods for Partial Differential Equations* (ed. R. G. Voigt, D. Gottlieb & M. Y. Hussaini), pp. 1–54. Philadelphia: SIAM.

GUCKENHEIMER, J. & HOLMES, P. 1983 *Nonlinear Oscillations, Dynamical Systems, and Bifurcations of Vector Fields*. Springer.

GUSTAVSSON, L. H. 1986 Excitation of direct resonances in plane Poiseuille flow. *Stud. Appl. Maths* **75**, 227–248.

HERBERT, T. 1975 On finite amplitudes of periodic disturbances of the boundary layer along a flat plate. In *Proc. Fourth Intl. Conf. on Num. Methods in Fluid Dynamics* (ed. R. D. Richtymer), Lecture Notes in Physics, vol. 35, pp. 212–217, Springer. (See also Res. Rep. DLR-FB 74–53.)

HERBERT, T. 1977 Die Neutralfläche der ebenen Poiseuillesströmung. Habilitationsschrift, Universität Stuttgart.

HERBERT, T. 1988 Secondary instability of boundary layers. *Ann. Rev. Fluid Mech.* **20**, 487–526.

Iooss, G. & Joseph, D. D. 1980 *Elementary Stability and Bifurcation Theory*. Springer.

Itoh, N. 1974 Spatial growth of finite wave disturbances in parallel and nearly parallel flows. Part 2. The numerical results for the flat plate boundary layer. *Trans. Japan Soc. Aerospace Sci.* **17**, 175–186.

Jang, P. S., Benney, D. J. & Gran, R. L. 1986 On the origin of streamwise vortices in a turbulent boundary layer. *J. Fluid Mech.* **169**, 109–123.

Jones, C. A. 1988 Multiple eigenvalues and mode classification in plane Poiseuille flow. *Q. J. Mech. Appl. Maths* **41**, 363–382.

Keller, H. B. 1977 Numerical solution of bifurcation and nonlinear eigenvalue problems. In *Applications of Bifurcation Theory* (ed. P. H. Rabinowitz), pp. 359–384. Academic.

Kleiser, L. & Zang, T. A. 1991 Numerical simulation of transition in wall-bounded shear flows. *Ann. Rev. Fluid Mech.* **23**, 495–537.

Koch, W. 1986 Direct resonances in Orr–Sommerfeld problems. *Acta Mech.* **59**, 11–29.

Laurien, E. & Kleiser, L. 1989 Numerical simulation of boundary-layer transition and transition control. *J. Fluid Mech.* **199**, 403–440.

Lifshits, A. M. & Shtern, V. N. 1986 Gauss method in nonlinear stability problems. In *Proc. Sixth GAMM Conf. on Numerical Methods in Fluid Mechanics* (ed. D. Rues & W. Kordulla), pp. 241–247. Vieweg & Sohn.

Lifshits, A. M., Rakhmatullaev, R. D. & Shtern, V. N. 1989 Threshold of development of three-dimensional structures in Blasius flow. *Fluid Dyn.* **24**, 515–520.

Likhachev, O. A. & Shtern, V. N. 1975 Self-oscillating flow in the boundary layer. *J. Appl. Mech. Tech. Phys.* **16**, 564–569.

Mahalov, A. & Leibovich, S. 1991 Weakly nonlinear analysis of rotating Hagen–Poiseuille flow. *Eur. J. Mech.* B: *Fluids* **10** (suppl), 55–60.

Milinazzo, F. A. & Saffman, P. G. 1985 Finite-amplitude steady waves in plane viscous shear flows. *J. Fluid Mech.* **160**, 281–295.

Morkovin, M. V. 1991 Panoramic view of changes in vorticity distribution in transition instabilities and turbulence. In *Boundary Layer Stability and Transition to Turbulence* (ed. D. C. Reda, H. L. Reed & R. Kobayashi). *ASME FED*, vol. 114, pp. 1–12.

Orszag, S. A. & Patera, A. T. 1983 Secondary instability of wall-bounded shear flows. *J. Fluid Mech.* **128**, 374–385.

Pugh, J. D. & Saffman, P. G. 1988 Two-dimensional superharmonic stability of finite amplitude waves in plane Poiseuille flow. *J. Fluid Mech.* **194**, 295–307.

Saffman, P. G. 1983 Vortices, stability and turbulence. *Ann. N.Y. Acad. Sci.* **404**, 12–24.

Schlichting, H. 1958 *Grenzschicht-Theorie* (3rd edn). Braun.

Schubauer, G. B. & Skramstad, H. K. 1948 Laminar boundary-layer oscillations and transition on a flat plate. *NACA Rep.* 909.

Sen, P. K. & Vashist, T. K. 1989 On the nonlinear stability of boundary-layer flow over a flat plate. *Proc. R. Soc. Lond.* A **424**, 81–92.

Shanthini, R. 1989 Degeneracies of the temporal Orr–Sommerfeld eigenmodes in plane Poiseuille flow. *J. Fluid Mech.* **201**, 13–34.

Smith, F. T. 1979*a* On the nonparallel flow stability of the Blasius boundary layer. *Proc. R. Soc. Lond* A **366**, 91–109.

Smith, F. T. 1979*b* Nonlinear stability of boundary layers for disturbances of various sizes. *Proc. R. Soc. Lond.* A **368**, 573–589 (and corrections *Proc. R. Soc. Lond.* A **371** (1980), 439–440).

Smith, F. T. 1988 A reversed-flow singularity in interacting boundary layers. *Proc. R. Soc. Lond.* A **420**, 21–52.

Smith, F. T. 1991 Nonlinear 3D interactions in open-flow transition. *Eur. J. Mech.* B *Fluids* **10** (suppl.), 301–306.

Smith, F. T. & Burggraf, O. R. 1985 On the development of large-sized short-scaled disturbances in boundary layers. *Proc. R. Soc. Lond* A **399**, 25–55.

Smith, F. T., Doorly, D. J. & Rothmayer, A. P. 1990 On displacement-thickness, wall-layer and mid-flow scales in turbulent boundary layers, and slugs of vorticity in channel and pipe flows. *Proc. R. Soc. Lond.* A **428**, 255–281.

SMITH, F. T. & KHORRAMI, F. 1991 The interactive breakdown in supersonic ramp flow. *J. Fluid Mech.* **224**, 197–215.

SOIBELMAN, I. & MEIRON, D. I. 1991 Finite-amplitude bifurcations in plane Poiseuille flow: two-dimensional Hopf bifurcations. *J. Fluid Mech.* **229**, 389–416.

SPALART, P. R. 1984 A spectral method for external viscous flows. *Contemp. Maths* **28**, 315–335.

STUART, J. T. 1960 On the nonlinear mechanics of wave disturbances in stable and unstable parallel flows. Part 1. The basic behaviour in plane Poiseuille flow. *J. Fluid Mech.* **9**, 353–370.